Received: 2 November 2018 | Revised: 3 January 2019 | Accepted: 14 January 2019

DOI: 10.1002/aoc.4847

WILEY Applied Organometallic Chemistry

FULL PAPER

Structural characterization, thermal investigation and biological activity of metal complexes containing Schiff Base ligand (Z)-3-(1-((4,6-dimethyl-1H-pyrazolo[3,4-b] pyridin-3-yl)imino)ethyl)-4-hydroxy-6-methyl-2H-pyran-2-one

Sanaa M. Emam | Saeyda A. Abouel-Enein | Eman M. Abdel-Satar

Chemistry Department, Faculty of Science, Menoufia University, Shebin El-Kom, Egypt

Correspondence
Eman M. Abdel-Satar, Chemistry Department, Faculty of Science, Menoufia University, Shebin El-Kom, Egypt.
Email: emanabdelsatar39@gmail.com

A new series of metal complexes containing Co(II), Pd(II), Fe(III) chloride and Cu(II) salts (chloride, bromide, sulphate and perchlorate) have been prepared with Schiff base ligand (**HL**). The synthesized compounds were elucidated using elemental analyses, spectral techniques, molar conductance, magnetic measurements and thermogravimetric studies. The analytical data established (1 M:1 L) stoichiometry for complexes (**1**), (**2**), (**4**), (**6**) and (**7**) as well as (1 M:2 L) and (2 M:3 L) stoichiometry for complexes (**5**) and (**3**), respectively. As a result, the ligand **HL** coordinates in complexes (**1**), (**2**), (**4**), (**6**) as a monobasic tridentate ONN moiety via the oxygen atom of the deprotonated phenolic OH, the nitrogen atoms of the azomethine and the imine group in pyrazolopyridine ring. While, it behaves as a neutral bidentate in complexes (**3**,**7**), chelates via oxygen and nitrogen atoms of enolic OH and azomethine groups. Also, in complex (**5**) Cu^{2+} ion binds via NO sits of two ligand molecules in its monobasic and neutral forms. The magnetic moment and electronic spectral data proposed octahedral structure for complexes (**2**, **3** and **7**) as well as triagonal bipyramidal and square pyramidal geometry for complexes (**1** and **4**), while, chelates (**5**) and (**6**) possess square planar geometry. TG/DTG studies confirmed the chemical formula for these complexes and established the thermal decomposition processes ended with the formation of metal or metal oxides contaminated with carbon residue. An axial electron spin resonance spectra were suggested for Cu(II) complexes pointing to $^{2}B_{1g}$ as a ground state with hyperfine structure for complex (**4**). In vitro antibacterial and antioxidant activities were performed for **HL** ligand and its metal complexes. The biological studies indicate that complex (**3**) has better antibacterial activity compared to the ligand and the other complexes.

KEYWORDS
biological studies, metal complexes, Schiff base, spectral techniques, thermal studies

1 | INTRODUCTION

Schiff base ligands have been employed intensively in analytical chemistry because of their excellent ability for complex formation with different metal ions. Also, this type of ligands is used as intermediates for the synthesis of some bioactive compounds. In addition, the ligands and their complexes depict antibacterial, antifungal, anticancer activities along with clinical and industrial uses.[1–11] Schiff bases are well used as antituberculosis, DNA binding and cleaving agents due to the existence of chelating azomethine group. On the other hand, the transition metal complexes are utlized for the synthesis of cancer combating nonradioactive tools for chemotherapy and diagnosis along with their uses in supramolecular photochemistry and in medicine.[12,13]

Dehydroacetic acid (DHA), 3-acetyl-6-methyl-2H-pyran-2,4(3H)-dione is one of the oxygen heterocyclic chelating agents and it is used for the synthesis of wide variety of heterocyclic ring systems.[14] DHA compounds have represented a permanent position in coordination chemistry that explores pharmacological and therapeutic activities.[15–17] Schiff bases derived from condensation of DHA with different amines, amino alcohols and amino phenols have various uses including analytical, clinical, biological and medicinal fields.[18–20] A number of metal complexes containing DHA and its Schiff bases have been reported to exhibit antitumor, antimicrobial, analytical, medicinal and supramolecular chemistry.[21–26] The biological activity associated with these chelates is ascribed to the presence of azomethine group (C=N).[27]

Fused heterocyclic systems containing pyrazole and pyridine rings have been attracted considerable attention due to their great usefulness in chemistry and a very wide spectrum of their biological activities. Pyrazolopyridines exhibit antitubercular, antiproliferative, inhibition of cyclin-dependent kinases and cardio-vascular antiviral and antileishmanial activities.[28–31] Pyrazolopyridines specially, pyrazolo[3,4-*b*]pyridine has proven to be interesting class of heterocycles due to diverse biological properties including antioxidant and antitumor activities.[32] This type of fused pryridines is isosters of bioactive indoles or indazoles[33] representing important building blocks in both natural and synthetic bioactive compounds.[34] Various pyrazolo[3,4-*b*]pyridines have been shown antimicrobial, antiviral and antiparastic activities[35–38] and also exhibit pharmacological properties such as anti-inflammatory, anxiolytic activity along with xanthine oxidase inhibitors, cholesterol formation inhibitor and anti-alzheimer. Also, pyrazolo[3,4-b]pyridines and their derivatives are attractive targets in organic synthesis ascribed to their biological activities such as analgesic, hypnotic, inhibitors of glycogen synthase kinase-3 (GSK-3), corticotrophin-releasing factor (CRF) antagonist, antidiabetic, antiarrhythmic. In addition, they are utilized as anti-HIV-1, potential glucocorticoid receptor ligand for positron emission tomography (PET).[39–41]

2 | EXPERIMENTAL

2.1 | Material and physical measurements

All chemicals used were chemically pure grade and were utilized without further purification. $CoCl_2.6H_2O$, $CuCl_2.2H_2O$, $CuBr_2$, $CuSO_4.5H_2O$, Cu $(ClO_4)_2.6H_2O$, $PdCl_2$ and $FeCl_3.6H_2O$ salts were used as received.

Elemental analyses (C, H, N) were performed on Perkin Elmer-2400 elemental analyzer at Main Defense Chemical Laboratory. All the metal ions of the prepared complexes were determined with Inductive Coupled Plasma Mass Spectrometry instrument (ICP), Perkin Elmer Model: Optima 7000 DV in solution. The solution of the investigated metal ions were prepared by decomposition (0.08 g) of complexes with concentrated HNO_3 mixed with concentrated HCl (*v*/v: 1:3), then followed by dilution with distilled water. While, the % of halide content (chloride or bromide) in the complexes was indirectly estimated by Mohr's method[42] after decomposition of the samples in concentrated nitric acid by boiling, followed by addition of distilled H_2O giving clear solution.

The infrared spectra were carried out on a Thermo-Fisher Nicolete FT-IR spectrophotometer within range (4000–400 cm^{-1}). The ^1H NMR spectra were measured in DMSO-d_6 on a DELTA-2 NMR spectrometer at 500 MHz, using tetramethylsilane (TMS) as internal reference. Fast Atom Bombardment (FAB) mass spectrum for the ligand was performed on a Shimadzu Qp-2010 Plus spectrometer. The electron spin resonance (ESR) spectra for Cu(II) complexes were performed on a Varian E-109c spectrometer equipped with a field modulation unit at 100 kHz. The measurements were done in the X–band with frequency 9.435 GHz on a microcrystalline powder at room temperature; the microwave power was around 10 mW. Perkin-Elmer Lambda 4B spectrophotometer was employed to measure the absorption electronic spectra in Nujol mulls. Molar conductivities of all metal complexes (except Pd complex) were measured in DMSO solution (10^{-3} M) at room temperature using a type CD6N Tacussel conductimeter; while it is measured in DMF solution for Pd(II) complex. The thermogravimetric analyses (TG/DTG) were carried out using a Shimadzu DAT/TG-50 thermal analyzer with a heating rate of 10 °C/min under N_2 atmosphere with a flowing rate of 20 mL/min from the room temperature up to 900 °C using platinum crucibles. Powder X-ray diffraction

patterns were measured using an X-ray diffractometer equipped with a graphite monochromator in the range (2θ = 5°-80°) by nickel separated CuK_α radiation (λ = 1.54060 A°).

Magnetic susceptibilities were measured at room temperature by Gouy method using a Johnson Matthey magnetic susceptibility balance. The diamagnetic corrections were calculated using Pascal's constants.[43] The effective magnetic moments were calculated as Bohr Magneton from the equation; $\mu_{eff} = 2.84(\chi_M^{corrt}\ T)^{1/2}$. The melting points were measured with Stuart melting point apparatus. Biochemical measurements antioxidant and antibacterial activities) were evaluated at Biotechnology Center, faculty of sciences, Mansoura University, Egypt.

2.2 | Synthesis of Schiff Base ligand; (Z)-3-(1-((4,6-dimethyl-1H-pyrazolo[3,4-b] pyridin-3-yl)imino)ethyl)-4-hydroxy-6-methyl-2H-pyran-2-one (HL)

The starting material, 4,6-dimethyl-1H-pyrazolo[3,4-b] pyridin-3-amine has been synthesized by the procedure published previously[44] and also, the preparation of a new ligand was carried out as shown in (Scheme 1). **HL** ligand was prepared by refluxing equimolar ratios of DHA (3.1 g) with 4,6-dimethyl-1H-pyrazolo[3,4-b] pyridin-3-amine (3.0 g) in 40 ml of hot absolute ethanol at 70 °C for 2 hrs. Then, few drops of DMF were added to the reaction mixture as a catalyst (dehydrating agent); it was further stirred under reflux at 70 °C for 3 hrs. The progress of the reaction was followed by TLC until all starting substances were completely reacted. The formed precipitate was filtered off, washed several times with hot ethanol and dried in a vacuum desiccator over anhydrous $CaCl_2$. The melting point of the ligand was found 230 °C.

2.3 | Synthesis of Schiff Base-metal complexes

Complexes (**1**–**7**) were synthesized by addition of (10 mmol) of the appropriate metal salt dissolved in absolute ethanol (15 ml) to a hot ethanolic solution (20 m) containing (20 mmol) of **HL** ligand. The reaction mixture was stirred under reflux for 5 hrs at 70 °C. The formed complex was filtered off, washed several times by boiling ethanol and dried under vacuum over anhydrous $CaCl_2$.

2.4 | Biological activity

2.4.1 | Antioxidant activity

The percentage of antioxidant activity (AA%) of **HL** ligand and its metal chelates

was determined by 2,2-diphenyl-1-picrylhydrazyl (DPPH•) free radical assay. The DPPH• radical scavenging activity was measured according to spectrophotometric methodology.[45] As a result of the delocalization of the DPPH• spare electron on the whole molecule, DPPH•

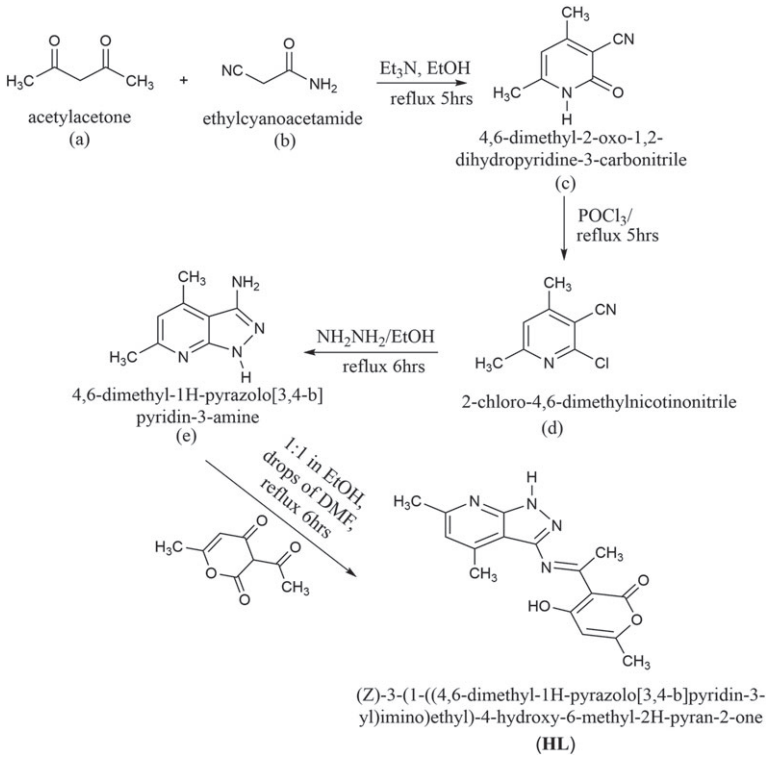

SCHEME 1 Synthesis of (HL) ligand

becomes a very stable free radical and not dimerize, as happens with most free radicals. The delocalization on the DPPH• molecule determines the occurrence of a deep violet color, and absorption occurs at about 517 nm. When DPPH• reacts with a hydrogen donor, the reduced form is generated, accompanied with the disappearance of the violet color. Therefore, the absorbance diminution depends linearly on the antioxidant concentration. Different concentrations of each investigated compounds were prepared and taken in separate test tubes. The volume was adjusted to 100 μL with methanol. Five mL of 0.1 mM methanolic solution of DPPH• was added to these tubes and shaken vigorously. The tubes were allowed to stand for 20 min at 27 °C. The samples were reacted with the stable DPPH• radical in methanol solution. The reaction mixture contains 0.5 ml of sample, 3 ml of methanol and 0.3 ml of DPPH• radical solution (0.5 mM) in methanol. DPPH• radical is reduced forming its molecule when it reacts with an antioxidant compound, which can donate hydrogen. Mixture of methanol (3.3 ml) and sample (0.5 ml) acts as blank. While, mixing of 3.5 ml of methanol and 0.3 ml of DPPH• solution affords the control solution and methanol was used for the baseline correction. The experiment was performed in triplicate for each compound and changes in the absorbance of the samples were measured.[46] After 100 min of reaction, the changes in color from deep violet to pale yellow were observed and read at 517 nm. Radical scavenging activity was expressed as the inhibition concentration (IC_{50}), i.e. the concentration of extract necessary to decrease the initial concentration of DPPH• by 50% (IC_{50}) under the specified experimental condition. The scavenging activity percentage (AA%) was determined according to the following equation[47]

$$AA\% = 100 - \frac{\left(Abs_{sample} - Abs_{blank}\right) \times 100}{Abs_{control}}$$

Where, $A_{control}$ = absorbance of DPPH radical + methanol and A_{sample} = absorbance of DPPH• + sample (test sample/standard).

2.4.2 | Antibacterial activity

The ligand **HL** and its metal complexes were tested in vitro antibacterial activity using the disc diffusion method,[48] against *E. Carotovora*, *P. Vulgaris* (Gram –ve bacteria); *B. Subtillis*, *S. areus* (Gram +ve bacteria). The antibacterial activity of each sample was estimated by paper disc diffusion assay using in inoculums containing 10^6 bacterial cells or 10^8 yeast cells/ml to be maintained on a nutrient and Czapek Dox agar plates, respectively. Thereafter, 25 ml of nutrient agar (medium) was poured into each petri plate and these plates were swabbed with the test organism and kept 15 min for adsorption. They were cultured at 37 °C for 18–24 hrs. The sterilized filter paper discs (6 mm in diameter) were saturated with infusion obtained from each sample and other set of filter paper discs were soaked in DMSO as control. The discs were placed on the surface of agar plates seeded with the tested organism. The plates were incubated at 37 °C for bacteria and diameters of inhibition zone (mm) were measured after 18–24 hrs because they were taken as measuring for antibacterial activity. Each treatment was replicated three times. The antibacterial activity of a common standard antibiotic (Streptomycin) was also estimated using the same procedure.

3 | RESULTS AND DISCUSSION

3.1 | Chemistry

The structure of **HL** ligand was identified using spectral methods (mass, ^{1}H NMR and infrared spectra). The Schiff base ligands containing DHA can exist in different tautomeric forms as, di-keto, keto-enamine and enol-imine forms[49] as shown in (Figure 1). An intramolecular hydrogen bridge binding one of the carbonyl groups (C^4=O) to the NH-moiety of the imine group was observed in (Figure 1b). Also, the intramolecular hydrogen bridge linking the azomethine group (C=N) to the protonated OH moiety was found to be a characteristic feature for **HL** ligand (Figure 1c and 1d). The six and four membered intramolecular hydrogen bonding rings are possible in the keto-enamine and enol-imine forms and observed in (Figure 1). The IR and ^{1}H NMR spectra confirmed the enol-imine form (Figure 1c).

3.2 | Characterization of Schiff base ligand (HL)

3.2.1 | Mass Spectrum (FAB)

FAB mass spectral data of Schiff base ligand (**HL**) (Figure S1) is carried out to restrict its molecular weight and study its fragmentation pattern. The important fragments obtained in its mass spectrum are shown in (Scheme 2). The mass spectrum displayed a molecular ion peak recorded at m/z = 332.18 peak corresponding to $[C_{16}H_{16}N_4O_3.H_2O]^+$. The loss of one water molecule giving a base peak at (m/z=313.21) which is equivalent to molecular weight (312.33) and molecular ion $[C_{16}H_{16}N_4O_3]^+$. Further, this base peak loss variable radicals affording fragment ion peaks recorded at m/z values

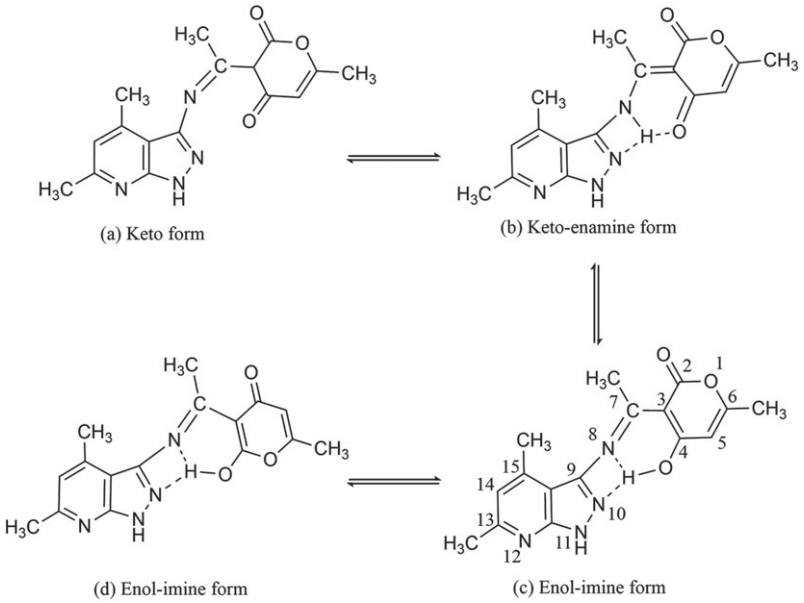

FIGURE 1 Tautomeric forms of HL Schiff base

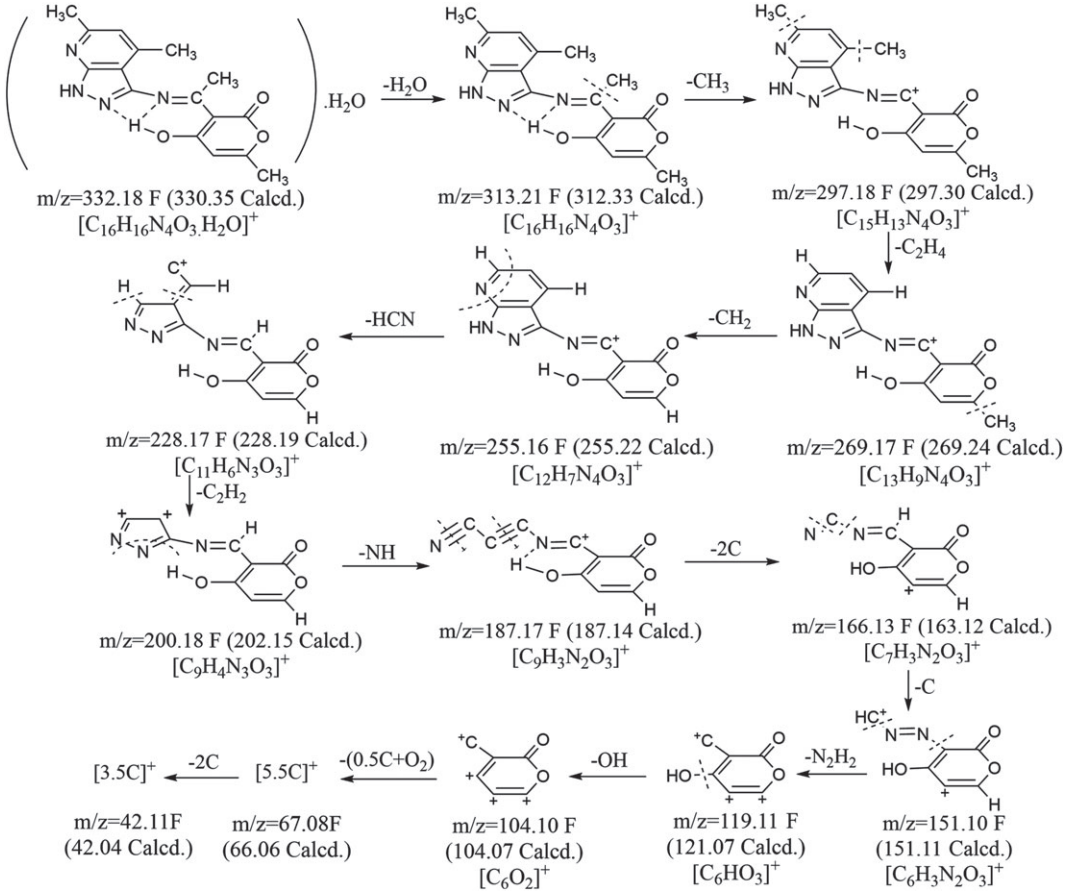

SCHEME 2 Proposed mass fragmentation of (HL) ligand

of 297.18; 269.17; 255.16; 228.17; 200.18; 187.17; 166.13; 151.11; 119.11; 104.1; 67.08 and 42.11 corresponding to $[C_{15}H_{13}N_4O_3]^+$; $[C_{13}H_9N_4O_3]^+$; $[C_{12}H_7N_4O_3]^+$; $[C_{11}H_6N_3O_3]^+$; $[C_9H_4N_3O_3]^+$; $[C_9H_3N_2O_3]^+$; $[C_7H_3N_2O_3]^+$; $[C_6H_3N_2O_3]^+$; $[C_6HO_3]^+$; $[C_6O_2]^+$; $[5.5C]^+$ and $[3.5C]^+$ fragment ions, respectively.

3.2.2 | ^{1}H NMR spectra of HL ligand and its Pd(II) complex

^{1}H NMR spectral data of **HL** ligand and its Pd (II) complex are listed in (Table 1) and shown in Figure (S2). ^{1}H NMR spectrum of Schiff base ligand in DMSO reveals

TABLE 1 ^{1}H NMR spectra of Schiff Base ligand and its palladium (II) complex

HL	[Pd(L)Cl].5H_2O*	Assignment
16.13	–	Enolic proton of –OH
13.61	12.80	NH proton
6.95	6.83	vinylic ^{14}C-H aromatic ring proton
5.87	6.06	vinylic ^{5}C-H aromatic ring proton
2.68	2.61	CH_3 protons of azomethine
2.53,2.56	2.53	CH_3 protons of P. P ring
2.15	2.49	CH_3 protons of DHA moiety (^{6}C-CH_3)
	3.75	Protons of crystallized water

p.p: pyrazolopyridine ring,

*DMF is used in ^{1} H NMR of $PdCl_2$ complex.

singlet signals at δ (16.13 and 13.61 ppm) attributed to protons of –OH and –NH, respectively.[50–52] It was found that the protonated OH peak is deshielded relative to the other OH protons, this is may be due to strong stabilization of the enolic form by intramolecular hydrogen bonding[53] (Figure 1c). While the singlet signals appeared at δ 6.95 and 5.87 ppm are denoted to two vinylic protons ^{14}C-H and ^{5}C-H, respectively.[51,52,54] Furthermore, the signals of protons of methyl groups attached to pyrane ring and azomethine group appear as sharp singlet at δ 2.15 and 2.68 ppm, respectively. While, the signals of protons of methyl groups attached with pyrazolopyridine moiety observed at δ 2.52–2.56 ppm.[31,55]

In the ^{1}H NMR spectrum of Pd(II) complex, the absence of protonated OH indicates the release of the OH proton and involvement of oxygen atom in binding with the metal ion after deprotonation of OH group. The up-field shift of NH proton may be due to its involvement in delocalization and its presence neighbor to nitrogen atom of cyclic $(C{=}N)_{p.p}$ group which is involved in coordination, this is confirmed with IR spectra. The methyl protons appeared at δ (2.49–2.61 ppm) on complexation. In addition, the spectrum of complex depicts a broad signal at δ (3.75 ppm) attributed to protons of crystallized water.[56]

3.2.3 | IR Spectrum of HL ligand

The IR spectrum of **HL** ligand (Table 2 and Figure S3) depicts most useful assignments for the characteristic bands. The IR spectrum of the ligand pointed to the absence of the bands characteristic to the amino group and carbonyl of acetyl group and instead, a new medium band due to azomethine (C=N) was appeared at1659 cm^{-1}.

This is indicative of the formation of Schiff base ligand (Scheme 1). The spectrum of the ligand displays spectral bands at (3451, 1156, 800); 1361 cm^{-1} cm^{-1} and (1311, 1258, 1199) cm^{-1}, assigned to protonated hydroxyl group (ν(OH), δ(OH), γ(OH)); ν(C–N) of arylazomethine, and phenolic ν(C–O), respectively.[14,21,23,56,57] These vibrational bands are taken as evidence for the presence of **HL** ligand in enol-imine form (Figure 1c) rather than

TABLE 2 Fundamental infrared spectral bands (cm^{-1}) of ligand (**HL**) and their assignments

Bands	Assignment	Bands	Assignment
3451(b, m)	$\upsilon(OH)_{enolic}$ + υ $(OH)H_2O$	1361(m)	υ(C-N) arylazomethine + CH_3 deformation
3220(w),3151(w)	$\upsilon(NH)_{P.P}$		
3092(w) 3015(w)	$\upsilon_{as}(C\text{-}H)_{aromatic}$ $\upsilon_{s}(C\text{-}H)_{aromatic}$	1311(m),1258(w) 1199(m)	$\upsilon(C\text{-}O)_{enolic}$
2939(m),	υ_{as}(C-H) of CH_3	1156(m)	δ(OH)
2925(m)		800(m)	γ(OH)
2855(w)	υ_{s}(C-H) of CH_3	1091(m), 945(s)	υ(N-N)
2798(w)	Hydrogen bonding	1065(m), 1030(w)	(C-H) in-plane bending
1722(s)	$\upsilon(C^2 = O)_{lactone}$	999 (w)	υ(C-O-C)
1659(m)	$\upsilon(C{=}N)_{azomethine}$	539(w)	$\gamma(C^2 = O)_{lactone}$
1603(s) 1571(s)	$\upsilon(C{=}C)_{cyclic\ ring}$ $\upsilon(C{=}N)_{Py}$	709(w)	γ(NH) + (C-H) out-of-plane bending
1497(m)	$\upsilon(C{=}N)_{P.P}$	621(w)	(C-H) in-plane bending of py
1462(w), 1442(w) 1402(w)	$\delta_{as}(C\text{-}H)\ CH_3$ $\delta_{s}(C\text{-}H)\ CH_3$	505(w)	$\rho(NH)_{P.P}$+(C–H) out-of-plane bending of py

Abbreviations: w: weak, m: medium, s: strong, b: broad, sh: shoulder, p.p: pyrazolopyridine, py: pyridine

TABLE 3 Analytical and Physical Data for Schiff Base Ligand (**HL**) and its Metal Complexes

No.	Compound	F.W. Color	Melting point (°C)	Elemental analysis Found/(Calcd.)% C	H	N	[a]X	M	*Λ_M
	$HL.H_2O$ $C_{16}H_{18}N_4O_4$	330.35 Off white	230	58.62 (58.17)	5.74 (5.49)	17.41 (16.96)	–	–	–
1	$[Co(L)Cl(H_2O(].0.5EtOH.3.75H_2O$ $C_{17}H_{27.5}N_4O_{8\cdot75}CoCl$	514.37 Dark green	200	39.90 (39.70)	5.73 (5.39)	11.18 (10.89)	6.77 (6.70)	11.54 (11.55)	28
2	$[Cu(L)Cl(H_2O)_2].EtOH.2.5\ H_2O$ $C_{18}H_{30}N_4O_{8.5}CuCl$	537.47 Brown	210	40.62 (40.23)	5.05 (5.60)	10.32 (10.42)	6.62 (6.60)	12.35 (11.81)	37
3	$[Cu_2(HL)_3Br_2(OH)(H_2O)]Br.6.5H_2O$ $C_{48}H_{64}N_{12}O_{17.5}Cu_2Br_3$	1456.13 Light brown	240	39.85 (39.59)	4.20 (4.43)	11.34 (11.54)	16.18 (16.48)	8.32 (8.72)	47
4	$[Cu(L)(OH)(H_2O)].0.25EtOH.0.5H_2O$ $C_{16\cdot5}H_{20.5}N_4O_{5.75}Cu$	430.37 Light green	185	46.36 (46.05)	4.25 (4.80)	13.90 (13.02)	-	14.30 (14.75)	17
5	$[Cu(HL)(L)]ClO_4.4.5EtOH$ $C_{41}H_{58}N_8O_{14.5}CuCl$	993.97 Yellowish green	246	49.59 (49.54)	5.12 (5.88)	11.95 (11.27)	-	6.48 (6.39)	48
6	$[Pd(L)Cl].5H_2O$ $C_{16}H_{25}N_4O_8PdCl$	543.32 Brown	280	35.06 (35.37)	4.76 (4.64)	11.01 (10.31)	6.91 (6.53)	19.64 (19.59)	10
7	$[Fe(HL)Cl(OH)_2(H_2O)].0.75EtOH.1.25H_2O$ $C_{17.5}H_{27}N_4O_8FeCl$	512.78 Light brown	235	40.61 (40.01)	11.31 (10.93)	4.65 (5.31)	6.48 (6.92)	11.20 (10.89)	14

*: ($\Omega^{-1}cm^2mol^{-1}$);

[a]: X = Chloride ion or bromide ion

TABLE 4 Infrared Spectral Bands (cm^{-1}) and their Assignments for Ligand **(HL)** and its Metal Complexes

No	Compound	$\upsilon(OH)^4$	$\upsilon(NH)^2$	$\upsilon(C^2{=}O)$	$\upsilon(C{=}C)$	$\delta(OH)$	$\upsilon(C^4{-}O)^4$	$\upsilon(N{-}N)$	$\upsilon(M{-}O)$	Other bands
		$\upsilon(OH)$ solvent	$\gamma(NH)^2$	$\upsilon(C{=}N)^5$ $\upsilon(C{=}N)^2$	$\upsilon(C{=}N)_{Py}$	$\gamma(OH){+}\delta(M{-}OH)$	$\upsilon(C{-}N)^3$	$\upsilon(C{-}O{-}C)$	$\upsilon(M{-}N)$	
	$HL.H_2O$	3451b,m	3220w 3151w 709m	1722 s 1659 m 1497m	1603 s 1571 s	1156m 800 m	1311m 1258sh 1199m 1361s	945m 1091w 999m	-	-
1	$[Co(L)Cl(H_2O)].0.5EtOH.3.75H_2O$	3411b,m 3126sh	3350sh 713w	1696 m 1654 w 1539 w	1607sh 1585 m	– – 779w*	1318w 1247w 1213w 1346w	966 m 1126w 1005 m	579 w 459 w	-
2	$[Cu(L)Cl(H_2O)_2].EtOH.2.5\ H_2O$	3550w 3423b.m 3321w	3136w 727w	1722 s 1631 s 1505 w	1605 sh 1572 s	– – 788w*	1303w 1242sh 1204 w 1364,1339m	950 w 1115 w 1000 w	537 w 487 w	-
3	$[Cu_2(HL)_3Br_2(OH)(H_2O)]Br.6.5H_2O$	3446m 3273w	3129w 727w	1722s 1664 w 1497w	1610 m 1573 s	1150w 805w 773w*	1309w 1273sh, 1220w 1368w	945m 1090w 999m	545 w 460 w	-
4	$[Cu(L)(OH)(H_2O)].0.\ 25EtOH.0.5H_2O$	3388m	3182w 708sh	1722s 1647w 1485w	1603 s 1573 s	1149 m 803w 882w*	1314w – 1202 m 1366w	951m 1081m 995w	539 w 485 w	-
5	$[Cu(HL)(L)]ClO_4.4.5EtOH$	3453m 3353m 3331sh	3154w 711w	1722s 1653 w 1631w 1497m	1596 m 1574 m	1151m 793w	1307w 1250w 1227w 1366w	945m – 999 m	550 w 470 w	(1089s, 626 m)[1]
6	$[Pd(L)Cl].5H_2O$	3523w 3450w	3182w 712 w	1714m 1634 s 1522 w	1591b.w	– –	1300w 1269 w 1216w 1343m	940w 1119m 999m	561 w 477 w	-

(Continues)

TABLE 4 (Continued)

No	Compound	$\upsilon(OH)^4$	$\upsilon(NH)^2$	$\upsilon(C^2{=}O)$		$\upsilon(C{=}C)$	$\delta(OH)$		$\upsilon(C^4{-}O)^4$	$\upsilon(N{-}N)$	$\upsilon(M{-}O)$	Other bands
		υ(OH) solvent	**γ(NH)²**	**υ(C=N)⁵**	**υ(C=N)²**	**υ(C=N)$_{Py}$**	**γ(OH)+δ(M–OH)**		**υ(C-N)³**	**υ(C-O-C)**	**υ(M-N)**	
7	$[Fe(HL)Cl(OH)_2(H_2O)].0.75EtOH.1.25H_2O$	3434b,m	3160w	1721 s		1603 s	1148m		1307w	945 m	585 w	-
			711w	1664 w		1574 s	807 m		1248w,	1091w	485 w	
				1497 m			737w*		1199m	999m		
									1366w			

[1]. (ClO_4^-) υ_4(1089(s), 947(s); υ_3(626 cm^{-1})),

[2]= p.p: pyrazolopyridine,

[3]: arylazomethine,

[4]: enolic,

[5]: azomethine,

*: coordinated water

Abbreviations: py: pyridine ring, w: weak, m: medium, s: strong, b: broad, sh: shoulder

di-keto and keto-enamine forms (Figure 1a, 1b, 1d).[58] The low value for protonated ν(OH) reveals its involvement in strong intramolecular hydrogen bonding as shown in Figure 1c. This is confirmed via its ^{1}H NMR spectrum.[59] Also, the IR spectrum (Table 2) indicates to the medium bands at (3220, 3151) and 709 cm^{-1} attributed to stretching and bending vibrations of pyrazolopyridine (NH) group.[54,60,61] On the other hand, the spectrum displayed asymmetric and symmetric stretching frequencies of aromatic and aliphatic (C–H) which are characterized by 3015–3092; 2925–2970; 2855 cm^{-1}, respectively.[53] But, the additional bands observed at (1462, 1442); 1402; (1065, 1030) cm^{-1} are restricted to asymmetric, symmetric bending vibrations of (CH_3) groups and aromatic (C–H) in-plane deformation.[62] Moreover, the **HL** spectrum exhibits strong and medium bands at (1722, 539); 1659; (1603,1571); 1497; (999) and (945, 1091 cm^{-1}) assignable to different vibrations of lactone carbonyl (C=O); ν(C=N) of azomethine group; (ν(C=C) + ν(C=N)) of pyridine; ν(C=N) of pyrazolopyridine; ν(C–O–C) of pyrane ring and ν(N–N), respectively.[49,56,63–65] Finally, the spectrum depicts weak to medium bands at 621 and 505 cm^{-1} which are denoted to (C–H) in-plain and out-of-plane bending of pyridine ring overlapped with ρ(NH) of pyrazolopyridine, respectively.[53,54,66]

3.3 | Characterization of Schiff Base metal complexes

3.3.1 | Analytical data

The physical and analytical results of **HL** ligand and its metal complexes are tabulated in (Table 3). The structure of the formed compounds was elucidated via microanalyses, spectral studies, thermal (TG/DTG), magnetic and molar conductance measurements. The metal complexes obtained from the reaction of **HL** ligand with different metal salts are separated with different stoichiometries. All metal complexes are stable, non-hydroscopic and partially soluble in aprotic organic solvents, but they are freely soluble in DMF and DMSO. The molar conductance values are recorded within range; 10–48 Ω^{-1} cm^2 mol^{-1}, revealing to non-electrolytic nature for complexes (**1**, **2**, **4**, **6** and **7**) along with 1:1 electrolyte for complexes (**3**) and (**5**).[67]

3.3.2 | IR spectra of metal complexes

FT-IR spectroscopy is a very useful tool in the characterization of Schiff base metal complexes. The IR spectral assignments of metal complexes are depicted in (Table 4

and Figure S4). The spectra of all chelates display broad medium bands in the region of (3321–3550 cm^{-1}) which may be pointed to ν (OH) of lattice solvent molecules/coordinated H_2O.[63] Besides, in the spectra of chelates (**1–4**) and (**7**), narrow weak bands at (779–882 cm^{-1}) specific for $\gamma(H_2O)$ rocking vibration of coordinated water molecules are also seen.[68–70]

The bands ascribed to ν(NH) and γ(NH) of pyrazolopyridine are displaced to lower/higher wavenumber in all metal complexes due to the predominant tautomeric form of these complexes and the involvement of adjacent (C=N) nitrogen atom in chelation with the metal ion. The strong lactone carbonyl band (1722 cm^{-1}) in the free ligand is found to be unaltered on complexation ruling out the participation of carbonyl oxygen in chelation with the metallic centers, while this band is shifted to lower wavenumber in complexes (**1**) and (**6**), this may be due to the existence of strong inter and intramolecular hydrogen bonding between carbonyl oxygen and hydrogen atom of lattice solvent molecules. Also, the ν(C=N) band assignable to azomethine group exhibits blue/red shift by (5–28 cm^{-1}) and appeared in a weak nature at (1631–1663 cm^{-1}) leading to its involvement in chelation via nitrogen atom in all complexes. This is supported by upward/downward shift in ν(C-N) values. While, the second band characteristic to ν(C=N) of pyrazolopyridine is positively and negatively shifted via (8–42 cm^{-1}) and (12 cm^{-1}) in complexes (**1**), (**2**), (**6**) and (**4**), respectively. Moreover, this band is unaltered in complexes (**3**), (**5**) and (**7**). This indicates that the (C=N) of pyrazolopyridine is one of the coordination sites in all complexes except complexes (**3**), (**5**) and (**7**), this is confirmed through the displacement of ligand ν(N–N) band (945, 1091 cm^{-1}) to higher/lower wavenumbers by (5–21), (10–35 cm^{-1}) in complexes (**1**), (**2**), (**4**) and (**6**).

The IR spectra of metal complexes (Table 4) display that the protonated ν(OH) is not clearly detected due to its overlapping with ν(OH) of lattice/coordinated solvent molecules. So, it is difficult to detect the shift in this band. While, the in-plane and out of plane bending vibrations (δ(OH), γ(OH)) bands of protonated OH appeared at (1156, 800 cm^{-1}) in the free ligand (Table 2) disappeared in complexes (**1**), (**2**), (**4**), (**6**), and the bands appeared at (1199, 1258, 1311 cm^{-1})assignable to ν(C–O) exhibit alteration in its shape and position with different degrees.[14] These observations indicate the involvement of phenolic (C–O) in coordination after deportation.[64] However, the free ligand bands (δ(OH) and γ(OH)) exhibit blue shift via (6–8 cm^{-1}) and red/blue shift via (5–22 cm^{-1}) in metal chelates (**3**) and (**7**). This behavior indicates the chelation of **HL** ligand through phenolic (–OH) group oxygen with Cu(II) and Fe(III) ions. These results reveal that **HL** ligand chelates with ions in monobasic tridentate manner via NNO type for complexes (**1**), (**2**), (**4**) and (**6**)), while, it behaves as neutral bidentate species in chelates (**3**) and (**7**) (NO fashion). This is supported by the existence of new bands in the range (537–585) and (459–485 cm^{-1}) attributed to ν(M–O) and ν(M–N),[55,58] respectively. In complexes (**3**), (**4**) and (**7**), new absorption bands appeared within range (3273–3446 cm^{-1}), may be assigned to ν(OH) of coordinated OH ion along with medium bands observed at (1148–1150) and (803–807 cm^{-1}) attributed to δ(OH) and γ(OH) of coordinated OH.[71–73]

The FT-IR spectrum of copper(II) perchlorate complex (**5**) revealed medium bands with high intensity within range (3331–3453 cm^{-1}) assigned to stretching vibration of coordinated (OH) group which is masked with that of lattice ethanol molecules. Moreover, the δ(OH), γ(OH) and ν(C–O) bands exhibited blue/red shift assisting the formation a bond between Cu(II) ion and oxygen atom of phenolic group. Also, the free ligand band (1659 cm^{-1}) assigned to ν(C=N) of azomethine group is splitted and shifted to lower wavenumbers (1653, 1631 cm^{-1}) accompanied with weak nature in complex (**5**), indicating the presence of two **HL** ligands chelated with Cu(II) ion through azomethine nitrogen atoms. This is supported by the red shift of arylazomethine (C–N), (Table 4). On the other hand, the second (C=N) band of pyrazolopyridine remains practically unaltered in frequency and the change in ν(N-N) is not observed, considering the noninvolvement of nitrogen atom of this group in chelation. Also, the existence of perchlorate ion is established by the appearance of strong band at 1089 cm^{-1} and medium band at 626 cm^{-1} assigned to $\upsilon_3(ClO_4)$ and $\upsilon_4(ClO_4)$. The lack of splitting of these bands show presence of non-coordinated perchlorate. Therefore, these values are matching with the molar conductance values (Table 3), indicating the presence of ionic perchlorate.[66,74–77]

The aforesaid changes in the IR spectral bands established that **HL** ligand behaves as a monobasic tridentate fashion through (NNO) type in complexes (**1**), (**2**), (**4**) and (**6**). While, **HL** chelated as (NO) type in complexes (**3**) and (**7**) with the metallic ions through nitrogen and oxygen atoms of azomethine group and phenolic –OH, respectively. But, the two ligands behaved as monobasic and neutral bidentate fashions via (NO) type in complex (**5**).

3.3.3 | Electronic spectra and magnetic moment measurements

The electronic spectra and magnetic susceptibility measurements have been used to determine the possible geometry of the prepared metal complexes. The electronic

spectra of **HL** ligand and its metal complexes were measured in Nujol mull at room temperature. The magnetic moment values and electronic absorption data are listed in (Table 5).

The spectrum of the ligand displays three bands, at 256, 301, 374 and 456 nm. The first, second and third bands are due to the electronic transition between anti-bonding orbitals (π–π*) of heterocyclic moiety, aromatic rings along with carbonyl and (C═N) groups.[58,78] The fourth band attributable to n–π* transition of conjugated system of the ligand.[79] The spectra of all metal complexes showed bands at 242–290 and 300–321 nm due to π–π*, while the electronic transition bands of n–π* show up at 422–438 nm.[80] The π–π* and n–π* transitions of the ligand suffered low shift upon complexation. All complexes display bands at (424–498 nm)

TABLE 5 Electronic spectral data and magnetic moments of the ligand and its metal complexes

No.	Compound	Spectral bands(nm)	Assignment	μeff. (B.M.) (per metal ion)
	HL. H_2O	256, 301 374 456	π-π* n-π*	–
1	$[Co(L)Cl(H_2O)].0.5EtOH.3.75H_2O$	246, 287 311,432 470 498 632 695	Intraligand transitions LMCT $^4A_2'(F) \rightarrow {}^4A_2'(P)$ $^4A_2'(F) \rightarrow {}^4E''(P)$ $^4A_2'(F) \rightarrow {}^4E'(F)$	4.80
2	$[Cu(L)Cl(H_2O)_2].EtOH.2.5H_2O$	242,316 368,432 468 528 572 670	Intraligand transitions LMCT $^2B_{1g} \rightarrow {}^2E_g$ $^2B_{1g} \rightarrow {}^2B_{2g}$ $^2B_{1g} \rightarrow {}^2A_{1g}$	1.79
3	$[Cu_2(HL)_3Br_2(OH)(H_2O)]Br.6.5H_2O$	246, 289 336,438 498 552 690	Intraligand transitions $^2B_{1g} \rightarrow {}^2E_g$ + LMCT $^2B_{1g} \rightarrow {}^2B_{2g}$ $^2B_{1g} \rightarrow {}^2A_{1g}$	1.12
4	$[Cu(L)(OH)(H_2O)].0.25EtOH.0.5H_2O$	246,268 300,355 466 540 721 769	Intraligand transitions LMCT $^2B_{1g} \rightarrow {}^2E_g$ $^2B_{1g} \rightarrow {}^2A_{1g}$ $^2B_{1g} \rightarrow {}^2B_{2g}$	1.80
5	$[Cu\ (HL)(L)]ClO_4.4.5EtOH$	248,290 321,422 466 670 714 786	Intraligand transitions LMCT $^2B_{1g} \rightarrow {}^2A_{1g}$ $^2B_{1g} \rightarrow {}^2E_g$ $^2B_{1g} \rightarrow {}^2B_{2g}$	1.72
6	$[Pd(L)Cl].5H_2O$	248,289 311 424 468 509	Intraligand transitions LMCT+$^1A_{1g} \rightarrow {}^1E_{1g}$ $^1A_{1g} \rightarrow {}^1B_{1g}$ $^1A_{1g} \rightarrow {}^1A_{2g}$	Diamagnetic
7	$[Fe\ (HL)Cl\ (OH)_2(H_2O)].0.75EtOH.1.25H_2O$	252,288 316,422 450 476 542 681	Intraligand transition LMCT $^6A_{1g}(S) \rightarrow {}^4A_{1g}(G), {}^4E_g(G)$ $^6A_{1g}(S) \rightarrow {}^4T_{2g}(G)$ $^6A_{1g}(S) \rightarrow {}^4T_{1g}(G)$	4.85

range, assignable to ligand to metal charge transfer (LMCT).[80]

In fact the μ_{eff} values for trigonal bipyramidal cobalt (II) complexes lie in the range 4.26–5.03 BM, owing to the orbital contribution of the excited (E') levels. The effective magnetic moment of (**1**) is (4.80 BM) as in some of the reported high-spin cobalt(II) complexes. This is because the orbital contribution to the spin-only value (3.87 BM) is fairly small, may be due to the presence of a low symmetry ligand field component with tetrahedrally distortion.[81,82] Cobalt(II) complex (**1**) displays electronic absorption bands at 498, 632 and 695 nm, assigned to $^4A_2$'(F) → $^4A_2$'(P), $^4A_2^{'}$'(F) → ^{4}E"(P) and $^4A_2^{'}$'(F) → ^{4}E'(F) transitions, respectively. These bands suggest a trigonal bipyramidal geometry for Co(II) complex.[72,81,82]

The spectra of Cu(II) complexes (**2**) and (**3**) exhibit bands at (498–528), (552–572) and (670–690) nm assigned to $^2B_{1g} \rightarrow {}^2E_g$, $^2B_{1g} \rightarrow {}^2B_{2g}$ and $^2B_{1g} \rightarrow {}^2A_{1g}$ transitions, respectively. These bands are consistent with octahedral geometry.[60,72,74,83] But, Cu(II) complex (**4**) shows bands at 540, 721 and 769 nm, corresponding to $^2B_{1g} \rightarrow {}^2E_g$, $^2B_{1g} \rightarrow {}^2A_{1g}$ and $^2B_{1g} \rightarrow {}^2B_{2g}$, indicating to square pyramidal structure for complex (**4**).[84–86] Also, the electronic spectrum of complex (**5**) depicts bands at 670, 714 and 786 attributed to $^2B_{1g} \rightarrow {}^2A_{1g}$, $^2B_{1g} \rightarrow {}^2E_g$ and $^2B_{1g} \rightarrow {}^2B_{2g}$ transitions affording square planar geometry for Copper(II) ion. The magnetic moment values of Copper(II) complexes are in the range (1.12–1.80 B.M) expected for distorted tetragonal structure around Cu(II) ion.[27,54,60,87] The lower magnetic moment value (1.12 B.M) for complex (**3**) pointes to the existence of interaction between Cu(II) ions, this is evidenced by the exchange coupling parameter (G) in its ESR spectrum.[66,74]

Diamagnetic Pd(II) complex displays three bands at 424, 468 and 509 nm assignable to $^1A_{1g} \rightarrow {}^1E_g$, $^1A_{1g} \rightarrow {}^1B_{1g}$ and $^1A_{1g} \rightarrow {}^1A_{2g}$, respectively, which is compatible with square planar stereochemistry.[72,74,87,88]

Iron(III) ion is usually high-spin in nearly all of its complexes, except those containing strongest ligands. The high-spin d^5 configuration of octahedral Fe(III) is expected to afford a magnetic moment, nearly equal to the spin-only value (5.90 B.M), where, the ground state has no orbital angular momentum. Lower values are reported for some hydroxo, chloro and bromo Fe(III) complexes due to the spin-crossover phenomenon.[89] It is to be noted that the magnetic moment value for complex (**7**) is (4.85 BM) implying high-spin octahedral structure around Fe(III) ion. The spectral bands of Fe(III) complex appear at 476, 542 and 681 nm corresponding to $^6A_{1g}(S) \rightarrow {}^4A_{1g}(G), {}^4E_g(G)$, $^6A_{1g}(S) \rightarrow {}^4T_{2g}(G)$ and $^6A_{1g}(S) \rightarrow {}^4T_{1g}(G)$ transitions indicative of high-spin octahedral geometry.[83,90]

3.4 | Thermal studies

Thermal analysis is a very useful technique in order to restrict the thermal stability of compounds, confirm molecular formulae and decide the different types of solvent of crystallization. This measurement is used to suggest a general mechanism for the thermal decomposition of these complexes. Figure (S5) represents TG/DTG curves of **HL** ligand and its complexes **(1–7)**. The TG curve of complexes reveal mainly three decomposition steps except complexes (**1**), (**4**) and (**7**) which undergo thermal degradation in four stages. The decomposition of all metal complexes initiated at low temperature (21–30 °C), this is may be due to the physically attached of the solvent of crystallization with the coordination sphere through inter/intramolecular hydrogen bonding. The final residue calculated from thermal decomposition is metal for complexes (**2–4** and **6**) and metal oxide contaminated with carbon for complexes (**1**, **5** and **7**). The structural properties of **HL** ligand, metal chelates, the different types of anions and the variety of the metal ions influence on the thermal behavior of the desolving/decomposition step in metal complexes, this studying can be explained by calculating the activation energy (*E**), the order of reaction (n), the activation enthalpy (ΔH*), the activation entropy (ΔS*) and the free energy of activation (ΔG*) using the analysis of the DTG curves. The order of reaction (n) can be determined from the relation: $(1-\alpha_m) = n^{(1-n)}$, where (α_m) is the decomposed fraction at DTG peak (the maximum rate of decomposition). The activation energy values of (*E**) for the desolvation/decomposition stage can be calculated using the initial rate method,[91,92] where, (*lnI*) is plotted versus (1000/T) for the low-temperature peak affording a straight line with a slop equals to (−E*/R), where *(I)* represents $(d\alpha/dt)$ in DTG curve and ΔT in DTA curve.[73,92,93] Also, the parameters (*ΔH*, *ΔS** and *ΔG*) were estimated from these relations: $\Delta H = E^* - R\Delta T$; $\Delta S^* = RTln\,(Ah/KT)$; $\Delta G = \Delta H - T\Delta S^*$, where *K, h, R, A and T* are Boltzmann's, Planck's and gas constants, frequency factor and absolute temperature, respectively. The thermal decomposition pathway of **HL** ligand and its metal complexes was studied by using TG analysis. The TG and DTG curves (Figure S5) together with the thermal results and their assignments are listed in (Table 6). So, the thermodynamic and kinetic parameters of the metal complexes are given in Table 7. The TG measurements were performed at a heating rate 10 °C/min under nitrogen within temperature range 21–900 °C.

The TG curve of ligand indicated that its thermal decomposition achieved through three steps. The first step takes place at temperature range 31–230 °C referring to small weight loss by 2.73% due to removal of 0.5 mol of

TABLE 6 Thermal analyses (TG/DTG) data for Schiff Base ligand (**HL)** and its metal complexes

No.	Compound	TG range (°C)	DTG Peak (°C)	Mass Loss% Calcd.	Mass Loss% Found	Assignment	T_s (°C)
	$HL.H_2O$	31–230		2.73	2.73	Loss of 0.5 mol of crystallized H_2O[a]	230
		230–280	261(s)	20.93	21.59	Loss of 0.5 mol of lattice H_2O and partial ligand pyrolysis (C_4H_{12})[c]	
		280–900		69.07	67.97	ligand pyrolysis ($C_{10}H_4N_4O_3$)[c]	
		At 900		7.27	7.71	(2C)[d]	
1	$[Co(L)Cl(H_2O)].0.5EtOH.3.75H_2O$	24–110	49(w)	3.11	2.95	Loss of 0.25 mol of EtOH and 0.25 mol of crystallized H_2O [1+2]	200
		110–200	163(br.w)	12.75	12.56	Loss of 0.25 mol of EtOH, 3 mol of crystallized H_2O [1+2]	
		200–330	229(br)	12.16	12.40	Loss of 0.5 mol of H_2O, one mol of coordinated H_2O and 0.5 mol of Cl_2 gas[c]	
		330–454	374(w)	15.57	16.26	Partial ligand pyrolysis (C_5H_4O)[c]	
		454–750	580(s.br)	31.73	31.28	Complete ligand pyrolysis ($C_8H_{11}N_4$)[c]	
		At 750		24.68	24.53	($Co_{2.54}O_4$+ 3C)[d]	
2	$[Cu(L)Cl(H_2O)_2].EtOH.2.5H_2O$	21–114	49(w)	3.81	3.18	Loss of 0.25 mol of EtOH and 0.5 mol of crystallized H_2O [1+2]	210
		114–210	170(m)	10.62	10.98	Loss of 0.75 mol of EtOH and 1.25 mol of crystallized H_2O [1+2]	
		210–310	270(w)	12.47	11.99	Loss of 0.75 mol of lattice H_2O, one mol of coordinated H_2O and 0.5 mol of Cl_2 gas[c]	
		310–776	697(m.br)	61.28	61.27	Complete ligand pyrolysis and loss of one mol of coordinated H_2O[c]	
		At 776		11.81	12.50	(Cu)[d]	
3	$[Cu_2(HL)_3Br_2(OH)(H_2O)]Br.6.5H_2O$	21–85				Stable zone	240
		85–176	142(w)	5.88	6.23	Loss of 4.75 mol of crystallized H_2O molecules[a]	
		176–240		2.17	2.25	Loss of 1.75 mol of crystallized H_2O molecules[a]	
		240–361	270(m)	10.98	10.69	Loss of one mol of Br_2 gas[c]	
		361–850	733(s.br)	72 25	72.17	Loss of one mol of coordinated H_2O, one mol of OH, 0.5 mol of coordinated Br_2 gas and 3 mol of HL ligand[c]	
		At 850		8.72	8.71	(2Cu)[d]	
4	$[Cu(L)(OH)(H_2O)].0.25EtOH.0.5H_2O$	25–185	47(w)	2.68	2.39	Loss of 0.25 mol of EtOH[b]	185
		185–304	253(m)280(s)	22.80	22.43	Loss of one mol of coordinated H_2O and partial ligand pyrolysis (C_5H_4O)[c]	
		304–410	380(s.br)	24.89	24.65	Loss of 0.5 mol of lattice H_2O, one mol of coordinated OH and partial ligand pyrolysis (C_5H_7N)[c]	

(Continues)

TABLE 6 (Continued)

No.	Compound	TG range (°C)	DTG Peak (°C)	Mass Loss% Calcd.	Mass Loss% Found	Assignment	T_s (°C)
		410–900	592(w)	34.88	35.78	Complete ligand pyrolysis ($C_6H_4N_3O_2$)[c]	
		At 900		14.75	14.76	(Cu)[d]	
5	[Cu (HL)(L)]ClO_4.4.5EtOH	23–194				Stable zone	246
		194–246	–	2.32	2.02	Loss of 0.5 mol of EtOH[b]	
		246–371	274(s)	22.76	22.22	Loss of 2.75 mol of lattice EtOH and one mol of ClO_4[c]	
		371–534	507 (m,br)	31.32	30.89	Loss of one mol of ligand ($C_{16}H_{15}N_4O_3$)[c]	
		534–700	572(m,br)	33.19	34.54	Loss of 1.25 mol of EtOH and ligand pyrolysis[c]	
		At 700		10.41	10.35	(CuO+ 2C)[d]	
6	[Pd(L)Cl].5H_2O	24–90	37(w)	3.32	3.10	Loss of one mol of crystallized H_2O[a]	280
		90–237		4.14	4.39	Loss of 1.25 mol of crystallized H_2O[a]	
		237–280	268(w)	9.12	9.17	Loss of 2.75 mol of lattice H_2O[a]	
		280–550	409(m,br)	63.83	63.72	Loss of 0.5 mol of Cl_2 gas and ligand pyrolysis[c]	
		At 550		19.59	19.64	(Pd)[d]	
7	[Fe (HL)Cl $(OH)_2(H_2O)$].0.75EtOH.1.25H_2O	25–104	44(w)	2.24	2.26	Loss of 0.25 mol of EtOH[b]	235
		104–235		4.49	4.38	Loss of 0.5 mol of EtOH[b]	
		235–300	277(s)	19.71	19.01	Loss of 0.75 mol of lattice H_2O, one mol of coordinated H_2O, two mol of coordinated OH and 0.5 mol of Cl_2 gas[c]	
		300–356	323(m,br)	15.23	15.60	Loss of 0.5 mol of lattice H_2O and partial ligand pyrolysis (C_4H_7N)[c]	
		356–600	400(s)	30.46	30.64	ligand pyrolysis ($C_{6.75}H_9N_3O_{1.5}$)[c]	
		At 600		27.87	28.12	($0.5Fe_2O_3$+ 5.25C)[d]	

Abbreviations:

[a]: dehydration

[b]:desolvation

[c]:decomposition,

[d]: final residue, T_S: thermal stability, s: strong; m: medium; w: weak and br: broad

crystal water molecule. The ligand starts its decomposition in the second step at 230–280 °C by weight loss 21.59% assigned to elimination of the rest of water molecule and partial ligand pyrolysis (C_4H_{12}). This process associated with strong DTG peak at 261 °C. Then, this step is followed by complete degradation at temperature range 280–900 °C with weight loss of 67.97% leaving carbon residue with 7.71%.

The TG curves of complexes (**2**), (**3**) and (**6**) reveal that they decompose by similar way. The initial desolvation step is observed through two processes at temperature ranges, 21–114, 114–210; 85–176, 176–240 and 24–90, 90–237 °C associated with weak to medium DTG peaks at 49,170; 142 and 37 °C for complexes (**2**), (**3**), and (**6**), respectively, (Scheme 3). Hence, the low temperature range for this transformation is indicative of the existence of releasing of adsorbed lattice solvent in chelated compounds. In this process, the ease of desolvation for these solvent molecules is ascribed to weak interaction in the crystal voids or no role in the lattice forces.[66,74,87,88,94] The calculated activation energies are found to be 75.99, 173.1; 75.91 and 140.72 KJmol^{-1} for complexes (**2**), (**3**) and (**6**), respectively. After that, the second decomposition step observed at temperature ranges (210–310), (240–361) and (237–300 °C) is accompanied by (T_{max} = 270, 270, 268 °C) with mass losses 11.99, 10.69

TABLE 7 Thermodynamic data of the thermal decomposition of Schiff Base ligand **HL** and its metal complexes

No.	Compound	DTG Peak(°C)	Temperature range (°C)	n	E*/KJmol^{-1}	ΔH*/KJmol^{-1}	A/s^{-1}	-ΔS*/Jmol^{-1}K^{-1}	ΔG*/KJmol^{-1}
	$HL.H_2O$	262	230–280	1.2	415.20	412.67	524.25	197.70	518.44
1	$[Co(L)Cl(H_2O)].0.5EtOH.3.75H_2O$	49	24–78	0.90	88.59	86.11	173.12	203.30	151.48
		163	110–200	1.58	24.86	22.15	32.81	219.04	118.06
2	$[Cu(L)Cl(H_2O)_2].EtOH.2.5H_2O$	49	21–114	1.17	75.99	73.48	146.25	204.10	141.71
		170	114–210	1.15	173.10	170.51	241.22	202.74	264.53
		270	210–308	1.34	121.68	118.91	133.69	209.18	232.50
3	$[Cu_2(HL)_3Br_2(OH)(H_2O)]Br.6.5H_2O$	142	85–200	1.21	75.91	73.07	105.33	208.94	162.62
		270	240–302	1.20	202.94	200.29	230.35	204.67	314.08
4	$[Cu(L)(OH)(H_2O)].0.25EtOH.0.5H_2O$	47	25–185	0.78	70.40	69.95	139.85	204.42	135.36
		253	185–266	1.54	130.92	128.08	149.58	207.99	237.49
		280	266–304	1.38	441.28	438.89	538.88	197.75	548.24
5	$[Cu\ (HL)(L)]ClO_4.4.5EtOH$	274	246–371	1.21	388.18	385.67	459.16	199.21	496.51
6	$[Pd(L)Cl].5H_2O$	37	24–90	1.09	140.72	138.34	307.34	198.21	199.72
		268	237–300	1.23	336.37	333.87	405.31	199.90	442.01
7	$[Fe\ (HL)Cl\ (OH)_2(H_2O)].0.75EtOH.1.25H_2O$	44	25–104	0.77	101.60	99.17	205.49	201.15	162.94
		277	250–300	1.42	474.95	472.61	592.77	197.70	580.05
		323	300–356	1.59	84.93	82.47	83.26	213.90	209.95

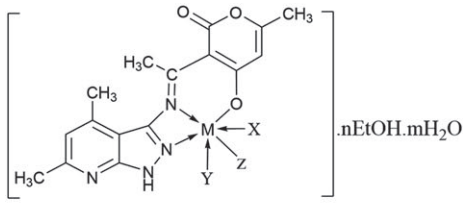

No.	M	X	Y	Z	n	m
(2)	Cu(II)	H_2O	H_2O	Cl^-	1	2.5
(6)	Pd(II)	-	-	Cl^-	-	5

(a) 21-237 °C | (2)-(EtOH+1.75H_2O) (6)-(2.25H_2O)

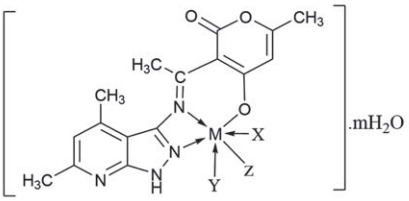

No.	M	X	Y	Z	m
(2)	Cu(II)	H_2O	H_2O	Cl^-	0.75
(6)	Pd(II)	-	-	Cl^-	2.75

(b) 210-310 °C | (2) -(1.75 H_2O+0.5 Cl_2) (6) -(2.75 H_2O)

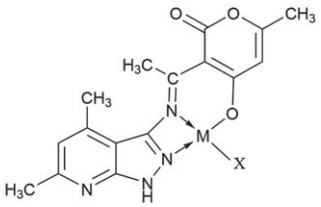

No.	M	X
(2)	Cu(II)	H_2O
(6)	Pd(II)	Cl^-

(c) 280-776 °C | (2) -(Ligand pyrolysis+H_2O) (6) -(Ligand pyrolysis+0.5Cl_2)

M

M= Cu, Pd

SCHEME 3 Thermal decomposition mechanism of complexes (2) and (6)

and 9.17% is assigned to removal of 0.75 mol of lattice H_2O molecule, 0.5 mol of Cl_2 gas along with removal of coordinated H_2O molecule for complex (**2**). The counted activation energies for this step are within range (121.68–336.37 KJmol^{-1}). But, this step corresponds to elimination of 0.5 mol of Br_2 gas and 2.75 mol of lattice water molecules for complexes (**3**) and (**6**), respectively. Finally, this step is followed by complete ligand pyrolysis for all complexes together with releasing of coordinated H_2O for complexes (**2**,**3**); coordinated anions (bromide and hydroxide) for complex (**3**) and coordinated chloride ion for complex (**6**). This step is accompanied with strong broad DTG peaks at (T_{max} = 697, 733,490 °C), ended with the formation of copper and palladium metals for complexes (**2**), (**3**) and (**6**), respectively.[72,74,88]

The thermoanalytical data showed that complexes (**5**) and (**7**) have isothermal behavior. The thermal decomposition proceeds in four steps within temperature range (194–700 °C) and (25–600 °C), where, Cu(II) complex shows no weight up to 194 °C. The first one (Schemes 4,5) occurs through one or two events within the temperature ranges (194–246 °C) and (25–235 °C) with weight losses 2.02% and 6.64%. This is pointing to partial desolvation with the removal of 0.5 and 0.75 mol of crystallized solvent for complexes (**5**) and (**7**), respectively. The thermal stability is observed up to 246 and 235 °C for complexes (**5**) and (**7**), respectively. After partial desolvation, the second decomposition stage takes place up to 371 and 300 °C assignable to removal of lattice EtOH molecules along with ionic perchlorate ion for complex (**5**) and elimination of lattice water, coordinated water molecule, chloride ion as well as coordinated hydroxyl for complex (**7**). This step is accompanied with sharp strong DTG peaks at (T_{max} = 274 and 277 °C) and the estimated activation energy for this step was found (388.18 and 474.95 KJmol^{-1}). The last degradation steps (third and fourth) in complexes (**5**) and (**7**) refer to loss of organic moieties at temperature ranges (371–700) and (300–600 °C) together with the remain lattice solvent molecules giving CuO and 0.5 Fe_2O_3 mixed with carbon.[54,57,66,72]

The thermal decomposition of complexes (**1**) and (**4**) shows four steps of releasing weight within temperature ranges (24–200), (185–330), (304–454) and (401–900 °C). The first decomposition step at (24–200 °C) is ascribed to partial desolvation with weight loss of 15.51 and 2.39% associated with weak DTG peak at (T_{max} = 49, 163 and 47 °C), respectively (Table 6; Scheme 6). On the other hand, this step is represented by two events with activation energy 88.59, 24.86 KJmol^{-1} and order of reaction 0.9, 1.58 for complex (**1**), while, this step is shown by single event with activation energy 70.40 KJmol^{-1} and first order reaction for complex (**4**) (Table 7). The complexes (**1**) and (**4**) begin the second degradation process at 200 and 185 °C up to 330 and 304 °C, respectively. This step is observed as one event with a broad DTG peak at (T_{max} = 229 °C) for complex (**1**) and two successive events with strong DTG peaks at (T_{max} = 253,280 °C) for complex (**4**). This was assigned to elimination of 0.5 mol of lattice H_2O molecule, one mol of coordinated H_2O molecule and 0.5 mol of Cl_2 gas for complex (**1**), in addition to partial ligand pyrolysis with coordinated H_2O in case of complex (**4**) (Table 6). When the temperature increases, within

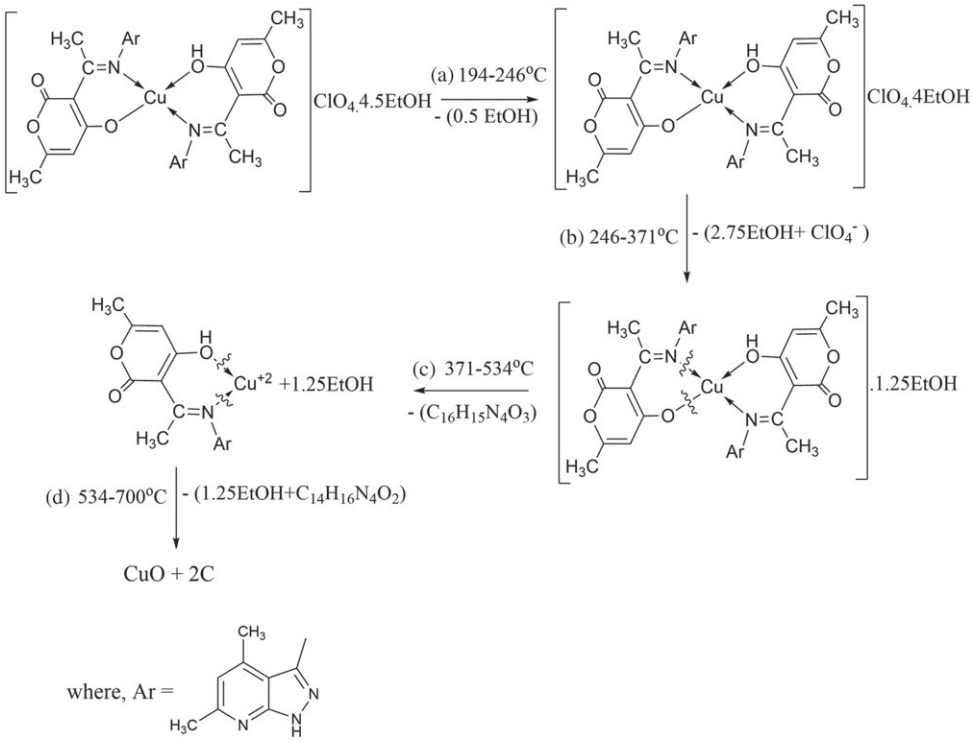

SCHEME 4 Thermal decomposition mechanism of complex (5)

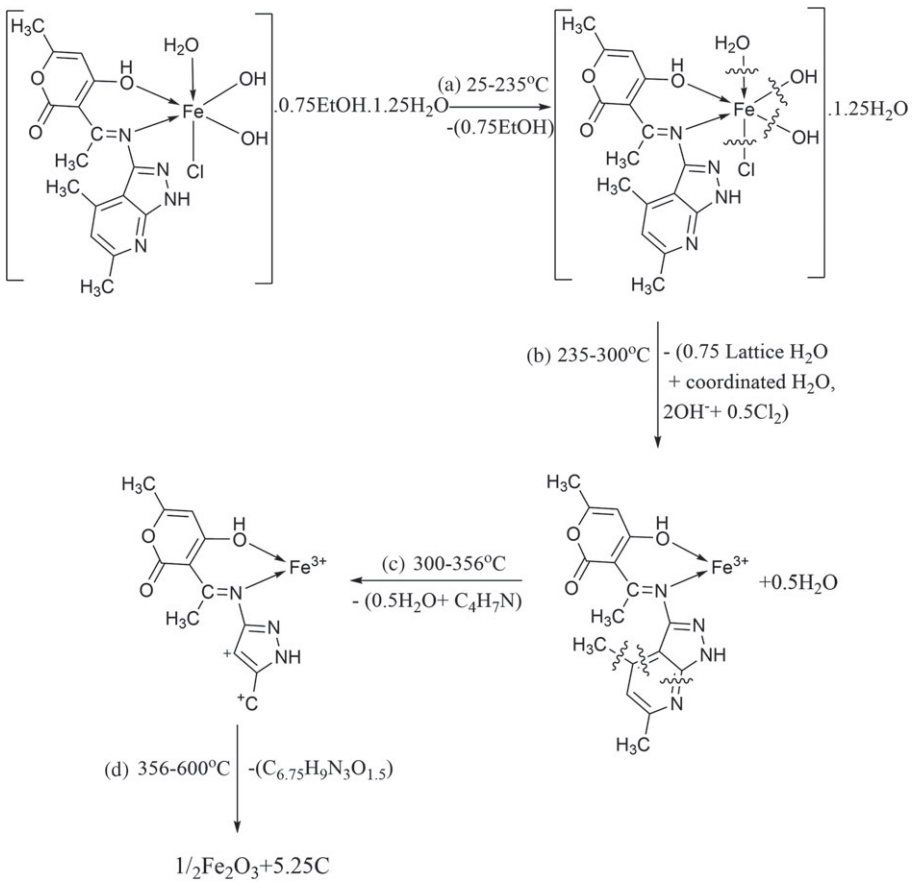

SCHEME 5 Thermal decomposition mechanism of complex (7)

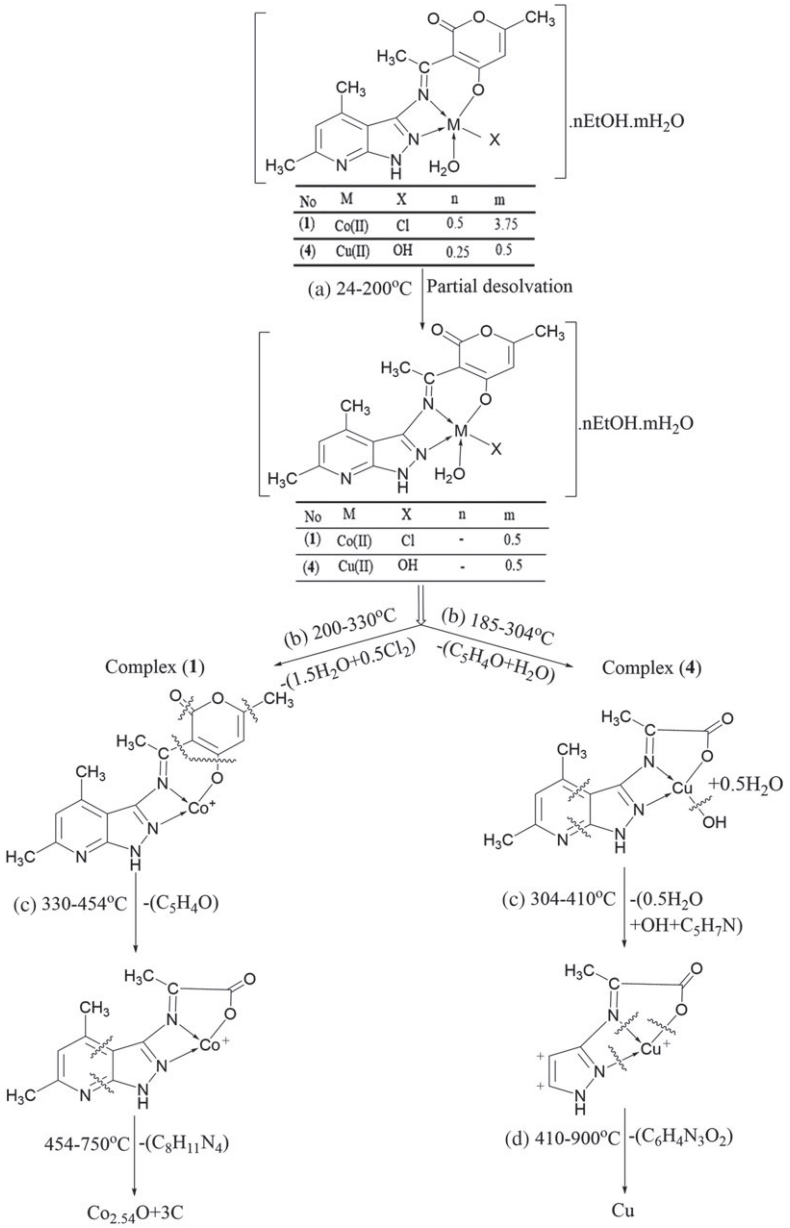

SCHEME 6 Thermal decomposition mechanism of complexes (1) and (4)

temperature ranges (330–750 °C), complete ligand pyrolysis takes place ending with the formation of cobalt oxide contaminated with carbon for complex (**1**), whereas, the removal of coordinated and lattice water along with complete delegation occurs for complex (**4**) within (410–900 °C) rang, and ended with copper metal as final residue[72,74,88] (Scheme 6, Table 6). The structure of cobalt oxide residue was illustrated using XRD diffraction pattern (Figure 2). It shows that no impurity peaks are observed, implying that the formed residue was pure $Co_{2.54}O_4$ and it is consistent with the card number (JCPDS 01–078-5623).[95] XRD pattern reveals all peaks intensities of (531), (440), (511), (400), (222), (311), (220) and (111), which can be perfectly indexed to diffraction angles (2θ in degree); 77.01, 64.95, 59.08, 44.48, 38.24, 36.50, 30.99 and 18.92, respectively. The crystallite size of the investigated $Co_{2.54}O_4$ oxide was calculated from the line broadening analysis of some diffraction lines utilizing Scherer equation[96]; ($D = K\lambda/\beta Cos\theta$), where ($K$), ($D$), ($\lambda$), ($\beta$) and ($\theta$) are Scherer's constant (0.90), the mean crystallite size (nm), the X-Ray wavelength (A°), full width half maximum (FWHM) of the oxide diffraction peaks and diffraction angle. The average crystallite size of this oxide was counted (39.05 nm).

3.5 | Kinetic and thermodynamic studies

Based on TG/DTG curves and the calculated thermodynamic parameters, the investigation of Tables 6 and 7 established these remarks:

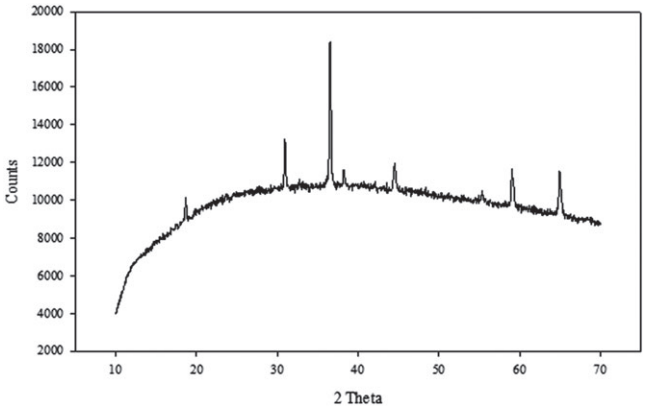

FIGURE 2 XRD pattern for cobalt oxide residue isolated from TG decomposition of complex (1)

- The Cu(II) perchlorate complex (**5**) has a higher thermal stability (start temperature of decomposition) than Cu(II) bromide complex (**3**). This may be due to the distribution of the ligand molecules around the central metal ion as shown in Figure 3, in addition to the different geometrical structures.[74] It was found that complex (**3**) has more steric effect than that observed for complex (**5**) (Figure 3). Also, the lower thermal stability of complex (**3**) is attributed to the strong repulsion between electrons of the two Cu(II) ions which has weakened on M–Br bond and facilitate the rupture of four membered ring in the first step decomposition reaction due to its exposed to torsional strain. This was confirmed by the higher activation energy value for the initial decomposition of complex (**5**) (388.18KJmol^{-1}) than that required for complex (**3**) (202.94 KJmol^{-1}).
- The higher thermal stability of square planar Cu(II) complex (**5**) (246 °C) than the distorted octahedral Cu(II) complex (**2**) (210 °C) may be due to the ionic character of complex (**5**) and the stronger interaction between Cu(II) ion with N_2O_2 chromophore in square planar Cu(II) complex (**5**) along with the increase in chelate rings around the central ion.[66,72]
- Table 7 demonstrates that the activation energy of desolvation step for complex (**2**) (75.99KJmol^{-1}) is greater than that observed for complex (**4**) (70.40KJmol^{-1}). This is attributed to the number and the nature of crystallized solvent molecules[68,87] which is confirmed with the higher thermal stability of complex (**2**) (T_s = 210 °C) than that of complex (**4**) (185 °C) (Table 6).
- The negative entropy values (ΔS*) of complexes for the thermal decompositions steps (Table 7), showed that the transition states are more ordered and the thermal reactions proceeded in complicated mechanisms.

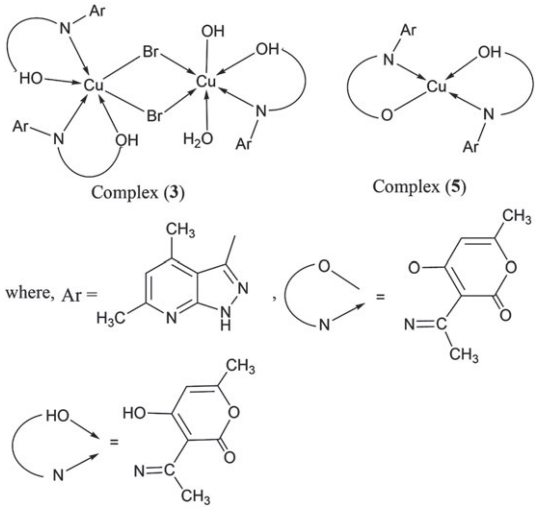

FIGURE 3 Distribution of chelate rings around Cu (II) ion in complexes (3) and (5)

3.6 | X-ray diffraction studies of metal complexes

The X-ray diffraction patterns of the prepared metal chelates (**3**), (**4**) and (**6**) are observed in curves a, b, and c of Figure 4, respectively. It is observed that Cu(II) bromide (**3**) and Cu(II) sulphate (**4**) complexes have polycrystalline nature. The X-Ray diffraction pattern of complex (**3**) is consistent with the peak positions in the (JCPDS cards, No. 00–064-1623, 01–082-2118, 01–076-5674) showing diffraction angles at 9.59, 11.47, 14.43, 16.40, 18.59, 23.46, 25.81, 27.09, 32.80, 36.73°. The low-angle reflection peaks at 11.47, 16.40, 25.81° can be found with d-spacing of 7.71, 5.37, 3.45 A°, which perfectly matched the reported interlayer spacing value for (C_2H_4(OH) NH_3CuBr_2). Whereas, the broad peak with very low intensity at around 27.09° was assigned to be the traces of CuBr with Cu(II) bromide. In addition, the weak intensity peaks at 18.59 and 25.81° matched with $C_9H_{14}O_7$ formula. The calculated crystallite size of complex (**3**) using Scherer equation was found (20.83 nm). Also, the XRD curve of complex (**4**) is consistent with the reported (JCPDS card, No. 01–073-4721), showing strong and weak diffraction peaks at 8.56, 9.35, 11.67, 14.32, 18.97, 23.33, 27.04, 28.72, 42.20 and 40.72° which perfectly matched with formula $(O_2CN(CH_3)_2)_2(NH\ (CH_3)_2)_2Cu$. The average crystallite size of this complex (**4**) exhibited a smaller average crystallite size of about 12.87 nm, than that of complex (**3**). While, Pd(II) complex (**6**) can have amorphous nature.

3.7 | Electron spin resonance studies

The ESR spectra of Copper(II) complexes (**2–5**) in the polycrystalline state were scanned at room temperature and the geometrical parameters were calculated. The data

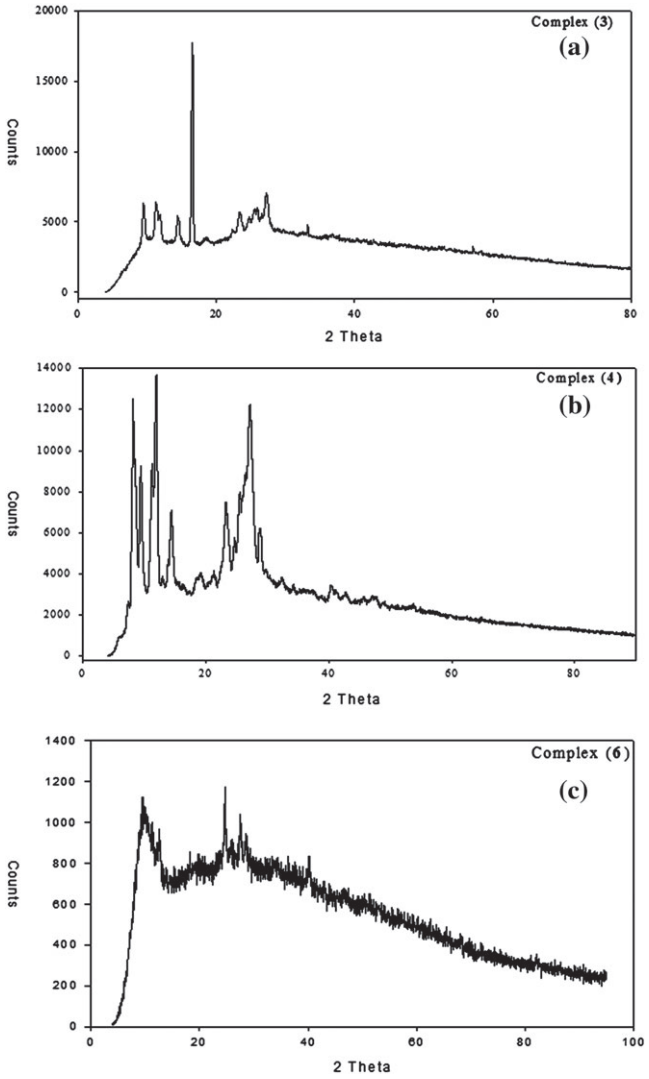

FIGURE 4 XRD curves for complexes (3), (4) and (6)

were listed in (Table 8) as well as the ESR curves for complexes (**2**) and (**4**) which are shown in Figure (S6). It was known that the Copper(II) ion have d^9 configuration with effective spin of ($s = 1/2$) and spin angular momentum of ($m_s = \pm 1/2$) creates a doubly degenerate spin state in the absence of external magnetic field. While the degeneracy of this state is lifted in the presence of a magnetic field and splitted to two spin energy levels with energy difference which is given by: $\Delta E = h\upsilon = g\beta H$, where ($h$) is Planck's constant, (υ) is the microwave frequency, (β) is Bohr magneton, (H) is the applied magnetic field and (g) is the land splitting factor for electronic transition from $m_s = +1/2$ to the other level of $m_s = -1/2$.

The ESR spectrum for complex (**2**) displays isotropic spectrum accompanied with (g) value of 2.12 and two broad signals with no hyperfine structure. It was concluded that the broadness of this peak is ascribed to dipolar interaction and a random orientation of

TABLE 8 ESR spectral parameters of Copper(II) complexes of **HL** ligand

Parameter	Complex (2)	Complex (3)	Complex (4)	Complex (5)
$g_{\|\|}$	–	2.870	2.199	2.530
$g_{\perp}$	–	2.130	2.051	2.094
[a] g_{av}/g_{iso}	2.12	2.380	2.10	2.240
[b] G	–	3.10	4.45	5.75
[c] $A_{//}$	–	–	147.70	–
[c] $A_{\perp}$	–	–	63.83	–
[d] A_{iso}	–	–	91.79	–
$K_{//}$	–	–	0.621	–
$K_{\perp}$	–	–	0.738	–
[e] K	–	–	0.699	–
α^2	–	–	0.668	–
β^2	–	–	0.578	–
γ^2	–	–	0.816	–
[f] f	–	–	148.89	–
[g] Δ_1	–	–	13004	–
[g] Δ_2	–	–	18519	–

[a] $g_{av} = \frac{g_{//} + 2g_{\perp}}{3}$
[b] $G = \frac{g_{//} - g_e}{g_{\perp} - g_e}$, $g_e = 2.0023$.
[c] = unit of A in (cm^{-1}).
[d] $A_{iso} = \frac{A_{//} + 2A_{\perp}}{3}$
[e] $K = \frac{K_{//} + 2K_{\perp}}{3}$
[f] $f = \frac{g_{//}}{A_{//}}$ in (cm).
[g] $\Delta_1 = {}^2B_{1g} \rightarrow {}^2B_{2g}$ (in cm^{-1}).
[g] $\Delta_2 = {}^2B_{1g} \rightarrow {}^2E_g$ (in cm^{-1}).

Copper(II) ion in addition to the interaction between the unpaired electron and the magnetic nuclei.[97]

Copper(II) complexes (**3**, **4**, **5**) depict axial spectra with two (g) values ($g_{||} = 2.199–2.87$, $g_{\perp} = 2.051–2.13$) associated with the trend $g_{||} > g_{\perp} > g_e$ indicating of $^2B_{1g}$ as ground state.[87,98] This is agreement with the electronic configurations $(eg)^4(b_{2g})^2$ $(a_{1g})^2$ $(b_{1g})^1$; $(eg)^4(a_{1g})^2(b_{2g})^2(b_{1g})^1$ and $(a_{1g})^2(eg)^4(b_{2g})^2(b_{1g})^1$ which are assignable to distorted octahedral, distorted square pyramidal and square planar geometry for complexes (**3**), (**4**) and (**5**), respectively.[98] In these chelates, the lowest (g)value is greater than (2.04) (Table 8), indicating to axial symmetry and all principle axes are aligned parallel with a (dx^2-y^2) ground state for square pyramidal geometry.[99–101]

The geometric parameter, *($G=g_{||}$-2/$g_{\perp}$-2)*, for this type of symmetry determines the exchange interaction between Cu(II) ions in the polycrystalline form. The observed value of this complex is equal to (4.45–5.75) suggesting the absence of copper-copper interaction in complexes (**4**) and (**5**).[87,102] Whereas, the calculated G value for complex (**3**)

was found (3.10) indicative of the existence of Cu-Cu interaction, this is in agreement with the lower value for its magnetic moment (μ_{eff} = 1.12BM). The ESR spectrum of complex (**4**) shows hyperfine splitting due to interaction between nuclear spin moment of Cu^{+2} ion (I = 3/2) and its electron spin moment (s = 1/2) in the parallel region. On the other hand a weak hyperfine splitting is observed in the high field region (Table 8). Also, the superhyperfine splitting due to coordinated nitrogen or oxygen is not shown for complex (**4**). The $g_{||}$, $A_{||}$, $g_{\perp}$ and $A_{\perp}$ values are listed in (Table 8). On the other hand, the empirical factor f ($f = g_{||}/A_{||}$) can be utilized to determine the stereochemistry of Cu(II) complexes. The (f) value is counted (148.89 cm) for complex (**4**) pointing to tetragonal distorted Copper(II) complexes.[74,92,103,104] In addition, the nature of metal–ligand bond is characterized by using the energies of d-d electronic transitions. The bonding parameters α^2, β^2 and γ^2 which are taken as measure of covalence of in-plane σ bonds, in-plane and out-of-plane π bonds; respectively will be calculated by these equations[90,104–106]:

$$\alpha^2 = \frac{A_{\|}}{0.036} + \left(g_{|} - g_e\right) + \frac{3(g_{\perp} - g_e)}{7} + 0.04$$

$$\alpha^2\beta^2 = K_{\|}^2 = \frac{(g_{\|} - g_e)\Delta_1}{8\lambda_0}$$

$$\alpha^2\gamma^2 = K_{\perp}^2 = \frac{(g_{\perp} - g_e)\Delta_2}{2\lambda_0}$$

Where λ◦ is the spin-orbit coupling constant for Cu(II), (α^2) indicates to the strength of (σ) bond between the ligand and Cu(II) ion, ($K_{||}$, $K_{\perp}$) are parallel and perpendicular components of orbital reduction factor and (Δ_1,Δ_2) are $^2B_{1g} \rightarrow {}^2B_{2g}$ and $^2B_{1g} \rightarrow {}^2E_g$, respectively. In our studied complex (**4**) ($\alpha^2 = 0.668$) indicating that the metal–ligand (σ) bond has slightly covalent character.[107]According to Hathaway,[108] K < 1 and $K_{||} < K_{\perp}$ assigned to in-plane π-bonding as well as greater covalent nature for metal–ligand bond. Also, the β^2 and γ^2 coefficients are less than unit attributed to the presence of in-plane and out-of-plane π character for metal–ligand bonds.[74]

Based on elemental analysis, spectral methods and thermal studies, the proposed structures for metal complexes are shown in Figure 5.

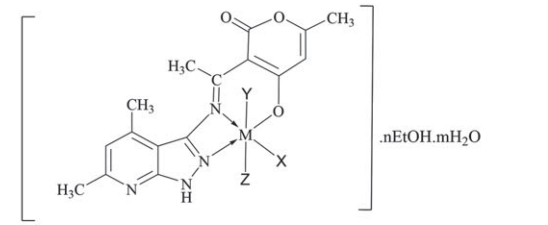

No.	Compound	M	X	Y	Z	n	m
1	[Co(L)Cl(H2O)].0.5EtOH.3.5H2O	Co(II)	Cl	H2O	-	0.5	3.5
2	[Cu(L)Cl(H2O)2].EtOH.2.5H2O	Cu(II)	Cl	H2O	H2O	1	2.5
4	[Cu(L)(OH)(H2O)].0.25EtOH.0.5H2O	Cu(II)	OH	H2O	-	0.25	0.5
6	[Pd(L)Cl].5H2O	Pd(II)	Cl	-	-	-	5

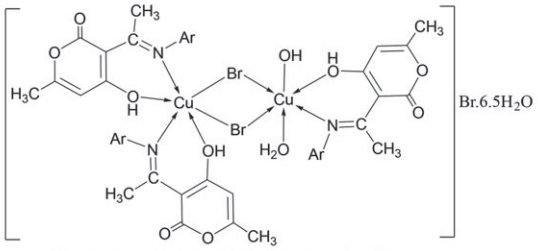

[$Cu_2(HL)_3Br_2(OH)(H_2O)$].6.5H_2O, Complex (**3**)

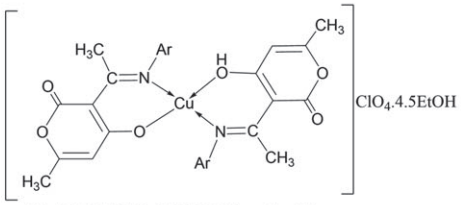

[Cu(HL)(L)]ClO_4.4.5EtOH, Complex (**5**)

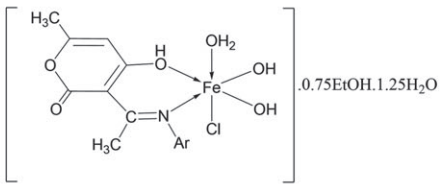

[Fe(HL)Cl$(OH)_2(H_2O)$].0.75EtOH.1.25H_2O, Complex (**7**)

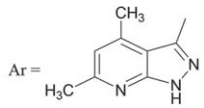

FIGURE 5 Proposed structures for metal complexes of (HL) ligand

3.8 | Biological activity

3.8.1 | Antioxidant activity

Antioxidants are molecules which inhibit or delay the oxidation of other molecules when they are found at low concentrations compared to those of an oxidizable substrate. The oxidation reaction produces free radicals implying to chain reactions which destroy cells. So, antioxidant prevents the initiation or propagation of oxidative chain reactions. In addition, the presence of antioxidants in food is very important for health-protection because they minimize the risk for chronic diseases including cancer and heart disease. The activity of a compound on the DPPH• radical is a fast and reliable parameter to measure the *in vitro* antioxidant activity of sample. This assay is based on the measurement of the decrease in molar

TABLE 9 In vitro antioxidant assay of **HL** ligand and its metal complexes using DPPH• method

No.	Compound	IC_{50}	Inhibition % Concentration mg/mL	
			0.009	0.004
	HL	0.0103	73.36	72.29
1	$[Co(L)Cl(H_2O(].0.5EtOH.3.75H_2O$	0.235	51.3	50.61
2	$[Cu(L)Cl(H_2O)_2].EtOH.2.5H_2O$	0.0211	65.95	60.23
3	$[Cu_2(HL)_3Br_2(OH)(H_2O)]Br.6.5H_2O$	0.156	52.80	–
4	$[Cu(L)(OH)(H_2O)].0.25EtOH.0.5H_2O$	0.076	55.9	47.63
5	$[Cu\ (HL)(L)]ClO_4.4.5EtOH$	0.078	56.90	50.99
6	$[Pd(L)Cl].5H_2O$	0.1337	45.43	–
7	$[Fe\ (HL)Cl\ (OH)_2(H_2O)].0.75EtOH.1.25H_2$	0.103	50.5	46.34
	Ascorbic acid	0.0221	–	–

All the concentrations in mg/ml at concentration 4.6 mg/ml

TABLE 10 In vitro antibacterial activity of **HL** ligand and its metal complexes

No.	Compound	Bacterial Strains			
		Erwinia carotovora	*Proteus vulgari*	*Bacillus stubtilis*	*Staphylococcus aureus*
		Diameter of the Growth Inhibition Zone, mm			
	HL	9	0	9	0
1	$[Co(L)Cl(H_2O(].0.5EtOH.3.75H_2O$	7	0	7	0
2	$[Cu(L)Cl(H_2O)_2].EtOH.2.5H_2O$	7	9	8	10
3	$[Cu_2(HL)_3Br_2(OH)(H_2O)]Br.6.5H_2O$	7	0	8	12
4	$[Cu(L)(OH)(H_2O)].0.25EtOH.0.5H_2O$	7	7	7	7
5	$[Cu\ (HL)(L)]ClO_4.4.5EtOH$	7	8	8	9
6	$[Pd(L)Cl].5H_2O$	7	0	7	0
7	$[Fe\ (HL)Cl\ (OH)_2(H_2O)].0.75EtOH.1.25H_2O$	7	0	0	6
	Control	6	0	7	0
	Streptomycin	12	8	12	12

absorptivity of DPPH• at (517 nm) after reaction with the tested compound. At the lowest concentration (20 μg/mL) the antioxidant activity of the free ligand was found to be (48.56%) but, upon complexation, it decreased significantly within the range (17.28% – 33%) (Table 9). It was observed, that the free ligand has higher activity than that of metal complexes but complex (**2**) has higher activity in comparison to the other complexes.[66]

3.8.2 | Antibacterial activity

Schiff base ligand (**HL**) and its metal complexes were tested for in *vitro* antibacterial against different pathogenic gram bacteria such as *Bacillus stubtilis*, *Staphylococcus aureus* and *Erwinia carotovora*, *Proteus vulgaris*, respectively. The inhibition zones were measured for the compounds, standard drugs (*Streptomycin*), control (DMSO) and tabulated in (Table 10). The results were compared relative to those of the standard, hence, (Table 10) revels that the Schiff base and its complexes show mild to moderate activity against these microorganisms. The results (Table 10) show that the ligand exhibits better antibacterial activity against *Erwinia carotovora* and *Bacillus stubtilis* than all investigated complexes.[10,66] The increase in biological activity of Schiff base is due to the presence of uncoordinated azomethine linkage (C=N).[109,110] According to the basis of Overton's concept and Tweedy's chelation theory,[109] the results showed that the complexes (**2**), (**4**), (**5**) are better antibacterial against *Proteus vulgaris* and Staphylococcus aureus than the inactive ligand. Also, the data depict that complex (**3**) is more active against

Staphylococcus aureus than complexes (**2**), (**4**), (**5**) and (**7**) relative to *Sterptomycin* (standard drug), while the other complexes (**1**, **6**) and the ligand do not exhibit activity against this type of bacteria. So, the resulted items of highest-to-lowest effective relative to *Staphylococcus aureus* can be summarized as follows:

$$(\mathbf{3}) > (\mathbf{2}) > (\mathbf{5}) > (\mathbf{4}) > (\mathbf{7})$$

4 | CONCLUSION

(Z)-3-(1-((4,6-dimethyl-1H-pyrazolo[3,4-b]pyridin-3-yl) imino)ethyl)-4-hydroxy-6-methyl-2H-pyran-2-one reacted with different metal salts to give the corresponding metal complexes with different stoichiometries. The suggested structures of the ligand and its complexes were proposed using physicochemical studies. The organic motif, **HL** binded in a monobasic tridentate manner in complexes (**1**), (**2**), (**4**) and (**6**) via deprotonated OH (pyranone ring) and nitrogen atoms of imine and pyrazolone (C=N) groups. While, it coordinated in a neutral bidentate form in complexes (**3**) and (**7**) via nitrogen and oxygen atoms of azomethine and OH groups. Also, one of the two ligands behaved as monobasic but the other reacts as neutral bidentate species in $Cu(ClO_4)_2$ complex via NO fashion type. The electronic spectra adopted triagonal bipyramid and octahedral structures for complexes (**1**) and (**2**), (**3**), (**7**), respectively. On the other hand, square pyramidal and square planar geometrical structures were suggested for complexes (**4**) and (**5**), (**6**), respectively. The ESR spectra of the Cu(II) complexes confirmed axial symmetry with $g\| > g\perp > 2.0023$, in agreement with a $^2B_{1g}$ ground state. The thermal stability of different metal chelates depends on the number of solvent molecules and steric factor. TG technique shows that the thermal decomposition process ended with the formation of metal or metal oxide mixed with carbon as final products. The antibacterial data demonstrated that complex (**3**) is more active against *Staphylococcus aureus*, while, the complexes (**2**), (**4**) and (**5**) are better antibacterial against *Proteus vulgaris* and *Staphylococcus aureus* than the ligand. Also, the antioxidant studies show that the ligand has better activity relative to the metal complexes.

ORCID

Sanaa M. Emam https://orcid.org/0000-0002-0680-5315
Saeyda A. Abouel-Enein https://orcid.org/0000-0002-5897-6896
Eman M. Abdel-Satar https://orcid.org/0000-0001-5184-1617

REFERENCES

[1] T. Rosu, E. Pahontu, C. Maxim, R. Georgescu, N. Stanica, G. L. Almajan, *Polyhedron* **2010**, *29*, 757.

[2] M. F. D. Karia, P. H. Parsania, *Asian J. Chem.* **1999**, *11*, 991.

[3] S. N. Pandeya, D. Sriram, G. Nath, E. De clercq, *Il Farmaco* **1999**, *54*, 624.

[4] A. H. El-masry, H. H. Fahmy, S. H. A. Abdelwahed, *Molecules* **2000**, *5*, 1429.

[5] A. K. Shaikh, M. A. Baseer, N. A. Mote, *Asian J. Chem.* **2001**, *13*, 496.

[6] P. G. More, R. B. Bhalvankar, S. C. Pattar, *J. Indian Chem. Soc.* **2001**, *78*, 474.

[7] S. B. Desai, P. B. Desai, K. R. Desai, *Heterocycl. Commun.* **2001**, *7*, 83.

[8] P. Phatak, V. S. Jolly, K. P. Sharma, *Orient. J. Chem.* **2000**, *16*, 161.

[9] I. P. Ejidike, P. A. Ajibade, *Molecules* **2015**, *20*, 9788.

[10] A. F. Shoair, A. A. El-Bindary, G. N. R. El-Ghamaz, *J. Mol. Liq.* **2018**, *269*, 619. https://doi.org/10.1016/j.molliq.2018.08.075

[11] H. A. Sahyon, A. A. El-Bindary, A. F. Shoair, A. A. Abdellatif, *J. Mol. Liq.* **2018**, *255*, 122.

[12] S. N. Pandeya, D. Sriram, G. Nath, E. DeClereq, *Eur. J. Pharm. Sci.* **1999**, *9*, 25.

[13] D. P. Sing, V. Malik, R. Kumar, K. Kumar, *J. Serb. Chem. Soc.* **2010**, *75*, 763.

[14] R. K. Pawar, M. A. Sakhare, B. R. Arbad, *Int. J. Chem. Sci.* **2016**, *14*, 2575.

[15] U. Kendur, G. H. Chimmalagi, S. M. Patil, K. B. Gudasi, C. S. Frampton, C. V. Mangannavar, I. S. Muchchandi, *J. Mol. Struct.* **2018**, *1153*, 299.

[16] E. S. Aazam, A. F. El Husseiny, H. M. Al-Amri, *Arab. J. Chem.* **2012**, *5*, 45.

[17] T. Punniyamurthy, S. J. S. Kalra, J. Iqbal, *Tetrahedron Lett.* **1995**, *36*, 8497.

[18] R. P. Saini, V. Kumar, A. K. Gupta, G. K. Gupta, *Med. Chem. Res.* **2014**, *23*, 690.

[19] B. M. Sharma, M. V. Parsania, A. J. Baxi, *Org. Chem. Indian J.* **2008**, *4*, 304.

[20] B. J. Gangani, P. H. Parsania, *J Spectrosc Lett* **2007**, *40*, 97.

[21] A. S. Munde, A. N. Jagdale, S. M. Jadhav, T. K. Chondhekar, *J. Serb. Chem. Soc.* **2010**, *75*, 349.

[22] S. M. Jadhav, A. S. Munde, S. G. Shankarwar, V. R. Patharkar, V. A. Shelke, T. K. Chondhekar, *J. Korean Chem. Soc.* **2010**, *54*, 515.

[23] S. Rahmouni, A. Djedouani, B. Anak, S. Tabti, A. Bendaas, M. Bencharif, M. François, S. Fleutot, F. Rabilloud, *J. Mol. Struct.* **2017**, *1148*, 238.

[24] S. R. Annapure, A. S. Munde, S. D. Rathod, *Der. Chem. Sinica* **2016**, *7*, 47.

[25] A. S. H. A. L. Alousi, M. R. Shehata, M. M. Shoukry, S. A. Hassan, N. Mahmoud, *J. Coord. Chem.* **2008**, *61*, 1906.

[26] K. C. Gupta, A. K. Sutar, *Coord. Chem. Rev.* **2008**, *252*, 1420.

[27] S. M. Emam, A. S. El-Tabl, H. M. Ahmed, E. A. Emad, *Synthesis, Arab J Chem* **2017**, *10*, S3816.

[28] D. U. Bawankule, K. Sathishkumar, K. K. Sardar, D. Chanda, A. V. Krishna, V. R. Prakash, S. K. Mishra, *J. Pharmacol. Exp. Ther.* **2005**, *314*, 207.

[29] F. A. Attaby, A. H. H. Elghandour, M. A. Ali, Y. M. Ibrahem, *Phosphorus Sulfur Silicon Relat. Elem.* **2006**, *181*, 1087.

[30] F. A. Attaby, A. H. H. Elghandour, M. A. Ali, Y. M. Ibrahem, *Phosphorus Sulfur Silicon Relat. Elem.* **2007**, *182*, 133.

[31] Y. K. Abdelmonem, F. A. El-Essawy, S. A. Abouel-Enein, M. M. El-Sheikh-Amer, *Int. J. Org. Chem.* **2013**, *3*, 198.

[32] U. Fathy, A. Younis, H. M. Awad, *J. Chem. Pharm. Res.* **2015**, *7*, 4.

[33] S. Kushwah, K. Prajapati, N. Darji, P. Soni, P. Shah, *Int. J. Pharm. Res. Bio-Sci.* **2012**, *1*, 287.

[34] E. Abdel-latif, S. Abdel-fattah, H. E. Gaffer, H. A. Etman, *Egyptian J. Basic Appl. Sci.* **2016**, *3*, 118.

[35] T. I. El-Emary, A. M. Kamal El-Dean, H. S. El-Kashef, *II Farmaco* **1998**, *53*, 383.

[36] A. M. R. Bernardino, A. R. de Azevedo, L. C. D. Pinheiro, J. C. Borges, V. L. Carvalho, M. D. Miranda, M. D. F. de Meneses, M. Nascimento, D. Ferreira, M. A. Rebello, V. A. G. G. da Silva, I. C. P. P. de Frugulhetti, *Med. Chem. Res.* **2007**, *16*, 352.

[37] T. I. El-Emary, S. A. Abdel-Mohsen, *Molecules* **2012**, *17*, 14464.

[38] A. M. R. Bernardino, H. C. Castro, I. C. P. P. de Frugulhetti, N. I. V. Loureiro, A. R. Azevedo, L. C. S. Pinheiro, T. M. L. Souza, V. Giongo, F. Passamani, U. O. Magalhaes, M. G. Albuquerque, L. M. Cabral, C. R. Rodrigues, *Bioorg. Med. Chem.* **2008**, *16*, 313.

[39] Z. Lu, G. R. Ott, R. Anand, R. -Q. Liu, M. B. Covington, K. Vaddi, M. Qain, R. C. Newton, D. D. Christ, J. Trazaskos, J. J. -W. Duan, *Bioorg. Med. Chem. Lett.* **2008**, *18*, 1958.

[40] M. A. Gouda, *Arch. Pharm. Chem. Life Sci.* **2012**, *345*, 155.

[41] S. A. Abdelmohsen, T. I. El-Emary, *Synthesis, J. Adv. Chem.* **2014**, *10*, 2901.

[42] J. Bassett, R. C. Denney, G. H. Jeffery, J. Mendham, *Vogel's Textbook, Quantitative Chemical Analysis*, 4th ed., Longman Group, London **1978**.

[43] J. Lewis, R. G. Wilkins, *Modern coordination chemistry, Principles and Methods*, Interscience, New York **1960** 403.

[44] F. A. Yassin, *Chem Heterocycl Compd* **2009**, *45*, 35.

[45] W. Brand-Williams, M. E. Cuvelier, C. C. Berset, *Lebensm. Wiss. Technol.* **1995**, *28*, 25.

[46] M. S. Blois, *Nature* **1958**, *26*, 1199.

[47] E. J. Garcia, T. L. C. Oldoni, S. M. de Alencar, A. Reis, A. D. Loguercio, R. H. M. Grande, *Braz. Dent. J.* **2012**, *23*, 22.

[48] A. W. Bauer, W. M. M. Kirby, J. C. Sherris, M. Turck, *Amer. J. Clin. Pathol.* **1966**, *45*, 493.

[49] S. Penta, *Introduction; In Dehydroacetic Acid and its Derivatives: Useful Synthons In Organic Synthesis*, 1st ed., Elsevier Science, National Institute of Technology, Raipur **2017**, 1.

[50] M. A. A. Elneairy, S. M. Eldine, A. S. I. Mohamed, *Der. Pharm. Chem.* **2015**, *7*, 284.

[51] A. S. Munde, A. N. Jagdale, S. M. Jadhav, T. K. Chondhekar, *J. Korean Chem. Soc.* **2009**, *53*, 407.

[52] A. K. Gupta, R. Pal, V. Beniwal, *World J. Pharm. Pharm. Sci.* **2015**, *4*, 990.

[53] S. Manivannan, S. Dhanuskodi, *J. Cryst. Growth* **2004**, *262*, 473.

[54] Y. K. Abdelmonem, S. M. Emam, H. M. Y. Okda, *J. Mater. Sci. Mater. Electron.* **2017**, *28*, 2923.

[55] A. K. Gupta, R. Pal, *World J. Pharm. Pharm. Sci.* **2015**, *4*, 386.

[56] S. M. Emam, S. A. Abouel-Enein, S. M. El-Seady, *J. Chin. Chem. Soc.* **2017**, *64*, 261.

[57] H. Ullah, F. H. Wattoo, M. H. S. Wattoo, M. Gulfraz, S. A. Tirmizi, S. Ata, A. Wadood, *Turk. J. Biochem.* **2012**, *37*, 386.

[58] S. M. Jadhav, V. A. Shelke, S. G. Shankarwar, A. S. Munde, T. K. Chondhekar, *J. Saudi Chem. Soc.* **2014**, *18*, 27.

[59] A. Z. El-Sonbati, M. A. Diab, A. A. El-Bindary, A. M. Eldesoky, S. M. Morgan, *Spectrochim. Acta A* **2015**, *135*, 774.

[60] D. G. Palke, S. D. Salunke, *Der. Pharm. Chem.* **2018**, *10*, 46.

[61] E. -S. A. El-Samanody, S. M. Emam, E. M. Emara, *J. Mol. Struct.* **2017**, *1146*, 868.

[62] S. A. Abouel-Enein, F. A. El-Saied, S. M. Emam, M. A. El-Salamony, *Spectrochim. Acta A* **2008**, *71*, 421.

[63] R. Gup, E. Giziroglu, B. Kırkan, *Dyes. Pigm.* **2007**, *73*, 40.

[64] N. Kavitha, P. V. A. Lakshmi, *J. Med. Chem.* **2016**, *8*, 184.

[65] N. Chitrapriyaa, T. S. Kamatchib, M. Zeller, H. Leea, K. Natarajan, *Spectrochim. Acta A* **2011**, *81*, 128.

[66] D. K. Sau, R. J. Butcher, S. Chaudhuri, N. Saha, *Polyhedron* **2004**, *23*, 5.

[67] S. M. Emam, S. A. Abouel-Enein, F. I. Abouzayed, *Appl. Organomet. Chem.* **2017**, *4073*, 1.

[68] N. Noroozi-Pesyan, J. Khalafy, Z. Malekpoor, *Prog. Color Colorants Coat.* **2009**, *2*, 61.

[69] A. Reiss, A. Samide, G. Ciobanu, I. Dăbuleanu, *J. Chil. Chem. Soc.* **2015**, *60*, 3074.

[70] K. P. Srivastava, A. Singh, S. K. Singh, *IOSR J. Appl. Chem.* **2014**, *7*, 16.

[71] A. Josephine, M. Teresita, A. Anantharaman, T. Rajasekar, J. Joesph, *Int. J. Pharm. Bio. Sci.* **2017**, *8*, 224.

[72] K. B. Gudasi, R. S. Vadavi, R. V. Shenoy, M. S. Patil, S. A. Patil, M. Nethaji, *Transition Met. Chem.* **2005**, *30*, 661.

[73] S. M. Emam, *J. Mol. Struct.* **2017**, *1134*, 444.

[74] K. Nakamoto, *Infrared Spectra of Inorganic Compounds*, 2nd ed., Wiley, New York **1970**.

[75] S. M. Emam, I. E.- T. El Sayed, M. I. Ayad, H. M. R. Hathout, *J. Mol. Struct.* **2017**, *1146*, 600.

[76] A. Z. El-Sonbati, M. A. Diab, A. A. El-Bindary, G. G. Mohamed, S. M. Morgan, M. I. Abou-Dobara, S. G. Nozha, *J. Mol. Liq.* **2016**, *215*, 423.

[77] M. F. Rosenthal, *J. Chem. Educ.* **1973**, *50*, 331.

[78] a V. L. Borde, S. G. Shankarwar, C. D. Thakur, A. G. Shankarwar, *Adv. Appl. Sci. Res.* **2014**, *5*, 229. b R. C. Mauryaa, B. A. Malika, J. M. Mira, P. K. Vishwakarmaa, D. K. Rajaka, N. Jaina, *J. Coord. Chem. 5015*(68), 1.

[79] O. A. El-Gammal, E. A. Elmorsy, Y. E. Sherief, *Spectrochim. Acta A* **2014**, *120*, 332.

[80] H. Hosseini-Monfared, R. Bikas, J. Sanchiz, T. Lis, M. Siczek, J. Tucek, R. Zboril, P. Mayer, *Polyhedron* **2013**, *61*, 45.

[81] H. Koksal, M. Dolaz, M. Tümer, S. Serin, *Synth. React. Inorg. Met-Org Chem.* **2001**, *3*, 1141.

[82] N. V. Somov, F. F. Chausov, R. M. Zakirova, I. V. Fedotova, *Russ. J. Coord. Chem.* **2015**, *41*, 729.

[83] Y. K. Abdel-Monem, S. A. Abouel-Enein, S. M. El-Seady, *J. Mol. Struct.* **2018**, *1152*, 115.

[84] S. Regupathy, M. S. Nair, *J. Saudi Chem. Soc.* **2012**, *16*, 247.

[85] N. S. Bedowr, R. B. Yahya, N. Farhan, *J. Saudi Chem. Soc.* **2018**, *22*, 255.

[86] V. K. Chityala, K. S. Kumar, R. Macha, P. Tigulla, Shivaraj, *Bioinorg. Chem. Appl.* **2014**, *2014*, 691260.

[87] S. M. Emam, S. A. Abouel-Enein, E. M. Emara, *J. Therm. Anal. Calorim.* **2017**, *127*, 1611.

[88] S. A. Abouel-Enein, S. M. Emam, M. W. Polis, E. M. Emara, *J. Mol. Struct.* **2015**, *1099*, 567.

[89] M. Nihei, T. Shiga, Y. Maeda, H. Oshio, *Coord. Chem. Rev.* **2007**, *251*, 2606.

[90] S. M. Emam, S. A. Abouel-Enein, F. A. El-Saied, S. Y. Alshater, *Spectrochim. Acta A* **2012**, *92*, 96.

[91] Y. Kirsh, S. Yariv, S. Shoval, *J. Therm. Anal. Calorim.* **1987**, *32*, 393.

[92] A. M. A. Alaghaz, M. E. Zayed, S. A. Alharbi, R. A. A. Ammar, *J. Mol. Struct.* **2015**, *1087*, 60.

[93] G. O. Piloyan, I. D. Ryabchikov, O. S. Novikova, *Nature* **1966**, *212*, 1229.

[94] R. G. Chaudhary, H. D. Juneja, R. Pagadala, N. V. Gandhare, M. P. Gharpure, *J. Saudi Chem. Soc.* **2015**, *19*, 442.

[95] M. El Baydi, S. K. Tiwari, R. N. Singh, J.-L. Rehspringer, P. Chartier, J. F. Koenig, G. Poilerat, *J. Solid State Chem.* **1995**, *116*, 157.

[96] M. V. Kumar, S. Muthulakshmi, A. A. Paulfrit, J. Pandiarajan, N. Jeyakumaran, N. Pandiarajan, *Int. J. Chem. Tech. Res.* **2014**, *13*, 5174.

[97] S. Sasi, M. Sithambaresam, M. R. P. Kurup, H. -K. Fun, *Polyhedron* **2010**, *29*, 2643.

[98] B. J. Hathaway, *Struct. Bond.* **1984**, *57*, 55.

[99] P. B. Sreeja, M. R. P. Kurup, A. Kirhore, C. Jasmin, *Polyhedron* **2004**, *23*, 575.

[100] B. J. Hathaway, A. A. G. Tomlinson, *Coord. Chem. Rev.* **1970**, *5*, 1.

[101] C. R. K. Rao, P. S. Zacharias, *Polyhedron* **1997**, *16*, 1201.

[102] B. J. Hathaway, J. N. Bradley, R. D. Gillard (Eds), *Essays in Chemistry*, Academic Press, New York **1971**, 61.

[103] O. Rojloo, F. Nourian, R. Arabahmadi, S. Aman, *Quim Nova* **2015**, *38*, 1187.

[104] H. A. El-Boraey, S. M. Emam, D. A. Tolan, A. M. El-Nahas, *Spectrochim. Acta A* **2011**, *78*, 360.

[105] U. Sakaguchi, A. W. Addison, *J. Chem. Soc. Dalton Trans.* **1979**, 600.

[106] S. M. Emam, I. E. T. El Sayed, N. Nassar, *Spectochim Acta A* **2014**, *138*, 942.

[107] B. J. Hathaway, *Structure and Bonding*, Vol. 14, Springer-Verlage, Heideberg **1973**, 49.

[108] D. Kivelson, R. Neiman, *J. Chem. Phys.* **1961**, *35*, 149.

[109] R. S. Joseyphus, M. S. Nair, *Microbiology* **2008**, *36*, 93.

[110] V. B. Badwaik, A. S. Aswae, *Russ. J. Coord. Chem.* **2008**, *34*, 179.

SUPPORTING INFORMATION

Additional supporting information may be found online in the Supporting Information section at the end of the article.

How to cite this article: Emam SM, Abouel-Enein SA, Abdel-Satar EM. Structural characterization, thermal investigation and biological activity of metal complexes containing Schiff Base ligand (Z)-3-(1-((4,6-dimethyl-1H-pyrazolo[3,4-b] pyridin-3-yl)imino)ethyl)-4-hydroxy-6-methyl-2H-pyran-2-one. *Appl Organometal Chem*. 2019;e4847. https://doi.org/10.1002/aoc.4847